

RESEARCH

Open Access



# Enhanced hippocampal LTP but normal NMDA receptor and AMPA receptor function in a rat model of CDKL5 deficiency disorder

Laura Simões de Oliveira<sup>1,2</sup>, Heather E. O'Leary<sup>3,8</sup>, Sarfaraz Nawaz<sup>1,2,4,5</sup>, Rita Loureiro<sup>1,2</sup>, Elizabeth C. Davenport<sup>1</sup>, Paul Baxter<sup>1,6</sup>, Susana R. Louros<sup>1,2</sup>, Owen Dando<sup>1,2,6</sup>, Emma Perkins<sup>1,2</sup>, Julien Peltier<sup>7</sup>, Matthias Trost<sup>7</sup>, Emily K. Osterweil<sup>1,2</sup>, Giles E. Hardingham<sup>1,2,6</sup>, Michael A. Cousin<sup>1,2,5</sup>, Sumantra Chattarji<sup>1,2,4,5</sup>, Sam A. Booker<sup>1,2</sup>, Tim A. Benke<sup>3,8\*</sup>, David J. A. Wyllie<sup>1,2,5,9\*</sup> and Peter C. Kind<sup>1,2,5,9\*</sup>

## Abstract

**Background** Mutations in the X-linked gene cyclin-dependent kinase-like 5 (*CDKL5*) cause a severe neurological disorder characterised by early-onset epileptic seizures, autism and intellectual disability (ID). Impaired hippocampal function has been implicated in other models of monogenic forms of autism spectrum disorders and ID and is often linked to epilepsy and behavioural abnormalities. Many individuals with CDKL5 deficiency disorder (CDD) have null mutations and complete loss of CDKL5 protein, therefore in the current study we used a *Cdkl5*<sup>-/-</sup> rat model to elucidate the impact of CDKL5 loss on cellular excitability and synaptic function of CA1 pyramidal cells (PCs). We hypothesised abnormal pre and/or post synaptic function and plasticity would be observed in the hippocampus of *Cdkl5*<sup>-/-</sup> rats.

**Methods** To allow cross-species comparisons of phenotypes associated with the loss of CDKL5, we generated a loss of function mutation in exon 8 of the rat *Cdkl5* gene and assessed the impact of the loss of CDKL5 using a combination of extracellular and whole-cell electrophysiological recordings, biochemistry, and histology.

**Results** Our results indicate that CA1 hippocampal long-term potentiation (LTP) is enhanced in slices prepared from juvenile, but not adult, *Cdkl5*<sup>-/-</sup> rats. Enhanced LTP does not result from changes in NMDA receptor function or subunit expression as these remain unaltered throughout development. Furthermore, Ca<sup>2+</sup> permeable AMPA receptor mediated currents are unchanged in *Cdkl5*<sup>-/-</sup> rats. We observe reduced mEPSC frequency accompanied by increased spine density in basal dendrites of CA1 PCs, however we find no evidence supporting an increase in silent synapses when assessed using a minimal stimulation protocol in slices. Additionally, we found no change in paired-pulse ratio, consistent with normal release probability at Schaffer collateral to CA1 PC synapses.

\*Correspondence:

Tim A. Benke  
tim.benke@cuanschutz.edu  
David J. A. Wyllie  
david.j.a.wyllie@ed.ac.uk  
Peter C. Kind  
p.kind@ed.ac.uk

Full list of author information is available at the end of the article



© The Author(s) 2024. **Open Access** This article is licensed under a Creative Commons Attribution 4.0 International License, which permits use, sharing, adaptation, distribution and reproduction in any medium or format, as long as you give appropriate credit to the original author(s) and the source, provide a link to the Creative Commons licence, and indicate if changes were made. The images or other third party material in this article are included in the article's Creative Commons licence, unless indicated otherwise in a credit line to the material. If material is not included in the article's Creative Commons licence and your intended use is not permitted by statutory regulation or exceeds the permitted use, you will need to obtain permission directly from the copyright holder. To view a copy of this licence, visit <http://creativecommons.org/licenses/by/4.0/>. The Creative Commons Public Domain Dedication waiver (<http://creativecommons.org/publicdomain/zero/1.0/>) applies to the data made available in this article, unless otherwise stated in a credit line to the data.

**Conclusions** Our data indicate a role for CDKL5 in hippocampal synaptic function and raise the possibility that altered intracellular signalling rather than synaptic deficits contribute to the altered plasticity.

**Limitations** This study has focussed on the electrophysiological and anatomical properties of hippocampal CA1 PCs across early postnatal development. Studies involving other brain regions, older animals and behavioural phenotypes associated with the loss of CDKL5 are needed to understand the pathophysiology of CDD.

**Keywords** CDKL5, rat, hippocampus, synaptic plasticity, intrinsic properties, AMPA receptor, NMDA receptor

## Background

Mutations in the X-linked gene cyclin-dependent kinase-like 5 (*CDKL5*; MIM: 300,203) cause a severe neurological disorder, estimated to affect 1 in 40,000 to 1 in 60,000 live births [1]. Patients present with early onset seizures, sleep disturbances, motor impairments, autistic features and severe intellectual disability (ID) [1, 2].

Pathogenic mutations are predicted to result in loss of protein function and predominantly cluster in the catalytic domain of CDKL5 [3], which is highly conserved across mice, rats and humans [4, 5]. Identification of physiological substrates of CDKL5 has suggested a role in cytoskeleton organisation [6, 7] which appears to be NMDA receptor dependent [7]. In line with this role in cytoskeleton organisation, reduced dendritic complexity and altered spine distribution have been repeatedly reported in *Cdkl5*<sup>-/-</sup> mice [8–11]. These anatomical phenotypes are frequently associated with altered synaptic function. Altered cellular and synaptic physiology has been reported in the hippocampus of a variety of mouse models of CDKL5 deficiency disorder (CDD). Altered long-term potentiation (LTP) has been observed in the hippocampus [12] and cortex [8] of *Cdkl5*<sup>-/-</sup> mice, with suggested mechanisms including an increase in calcium-permeable (CP) AMPA receptors [13] and NMDA receptor dysfunction [12, 14]. These phenotypes are thought to underlie hippocampal-dependent learning and susceptibility to chemically induced seizures [11, 12, 15].

NMDA receptor activation during development is known to influence synapse numbers and dendritic arborisation [16]. Moreover, NMDA receptor subunit composition undergoes a developmental switch and has an important role in regulating AMPA receptor presence at synapses [17]. As such it is important to assess the development of NMDA receptor subunit expression in preclinical models of CDD. In fact, the role of CDKL5 in synaptic function during early postnatal development and juvenile stages is unknown, as most studies so far have focused on adult mice. Moreover, with conflicting reports from a variety of mouse models it is imperative to identify robust physiological phenotypes that cross the species barrier in order to identify disease mechanisms and therapeutic strategies which might translate to the human condition. In the current study, we address this issue using a rat model of CDD to allow a cross-species

comparison of the reported pathophysiology associated with the loss of CDKL5. We hypothesised that loss of CDKL5 leads to impaired synaptic function in the hippocampus of *Cdkl5*<sup>-/-</sup> rats. We examined synaptic physiology and plasticity alongside cellular morphology using a combination of extracellular and whole cell electrophysiological recordings and histology. Whilst we found increased hippocampal LTP in *Cdkl5*<sup>-/-</sup> rats, we found that NMDA receptors undergo a typical developmental trajectory and we do not observe an increase in CP-AMPA receptor mediated currents that could contribute to the enhanced LTP. We observe reduced mEPSC frequency accompanied by increased spine density in basal dendrites of CA1 PCs, however we find no evidence supporting an increase in silent synapses when assessed using a minimal stimulation protocol in slices. Additionally, we found no change in paired-pulse ratio, consistent with normal release probability in *Cdkl5*<sup>-/-</sup> rats. Overall, our data presents evidence supporting a role for CDKL5 in hippocampal synaptic function, however the underlying mechanisms are still unclear and appear to be distinct to those previously reported in mouse models of CDD.

## Methods

### Breeding and animal husbandry: Edinburgh and Bangalore

All procedures were performed in line with the University of Edinburgh and Home Office guidelines under the 1986 Animals (Scientific Procedures) Act, CPCSEA (Government of India) and approved by the Animal Ethics Committee of the Institute for Stem Cell Science and Regenerative Medicine (inStem).

### Breeding and animal husbandry: Colorado

All studies conformed to the requirements of the National Institutes of Health *Guide for the Care and Use of Laboratory Rats* and were approved by the Institutional Animal Care and Use subcommittee of the University of Colorado Anschutz Medical Campus (protocol 00411). All rodents were housed in micro-isolator cages with water and chow available *ad libitum*. Animals were bred in house on the Long Evans Hooded background and housed with littermates on a 12 h light/dark cycle with food and water *ad libitum*.

Experiments were performed on wild-type (WT; *Cdkl5*<sup>+/+</sup>) and *Cdkl5*<sup>-/-</sup> rats at post-natal day (P) 28 to 35

unless otherwise stated. All experiments and data analyses were performed blind to genotype.

**Cdkl5<sup>-/-</sup> rat generation and genotyping**

The *Cdkl5<sup>-/-</sup>* rat model was created using CRISPR/Cas9 technology to introduce a 10 bp (bp) deletion in exon 8 of the *Cdkl5* gene (Ensembl coordinates X:35,674,763–35,674,772, in the Rnor\_6.0 genome assembly). An in-house PCR-based strategy was designed to genotype experimental rats produced from crossing *Cdkl5<sup>-/-</sup>* males with WT females. Forward and reverse primers were

generated flanking the bp deletion site in exon 8 of the rat CDKL5 gene (F1 and R), a third forward primer which anneals to the 10 bp deletion site in the WT allele (F2) and a further forward primer which anneals over the deleted 10 base pairs in the knock out (KO) allele (F3) were also generated (Fig. 1).

F1: 5' -GGGCTTGTAGCAAATCCATCC- 3'  
 R: 5' -AGCAAGCAGAGTTCTATTTTCCT- 3'  
 F2: 5' -ATACGTGGCTACTCGGTGGTAC- 3'  
 F3: 5' -CAGAATACGTGGCTACCGATC- 3'

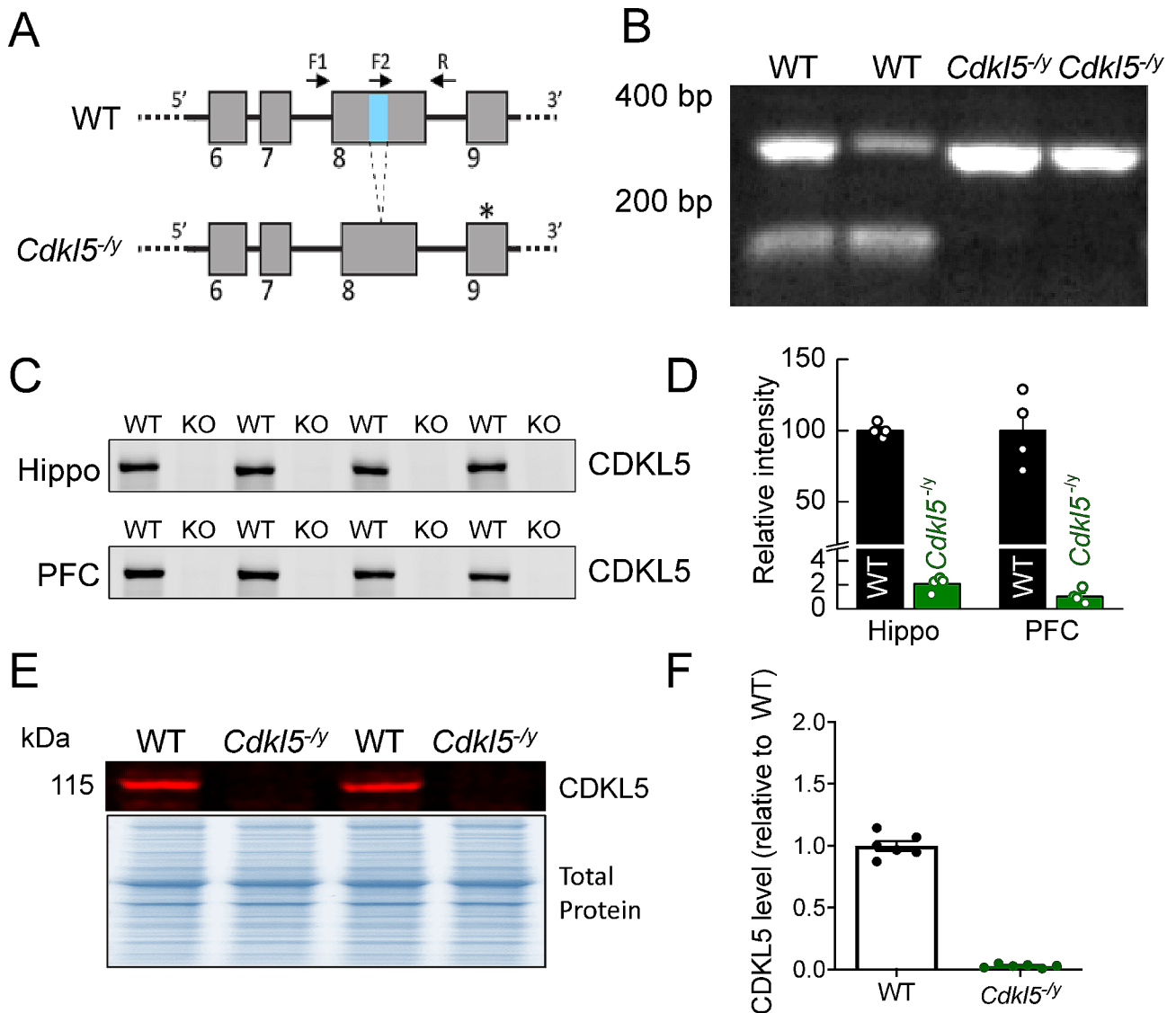


**Fig. 1** Validation of *Cdkl5<sup>-/-</sup>* rats. **(A)** Schematic of the *Cdkl5* knockout strategy depicting the WT and null alleles. The null allele has a 10 bp (bp) deletion in exon 8 (region shown in blue in WT allele), leading to a frame shift and an in frame, premature STOP codon forming in exon 9 (\*). **(B)** Genotyping results from male WT and *Cdkl5<sup>-/-</sup>* animals. Higher band in WT and *Cdkl5<sup>-/-</sup>* animals resulting from F1 and R primers product. Lower band in the WT samples resulting from F2 and R primer products is absent in the null samples due to the 10 bp deleted sequence. **(C)** Western blot showing the absence of CDKL5 in hippocampal and prefrontal cortex tissue preparations from WT and *Cdkl5<sup>-/-</sup>* rats. **(D)** Quantification of CDKL5 western blot protein expression in hippocampal and prefrontal cortex preparations. **(E)** Western blot showing the absence of CDKL5 in hippocampal synaptosome preparations from WT and *Cdkl5<sup>-/-</sup>* rats. **(F)** Quantification of CDKL5 western blot protein expression in hippocampal synaptosome preparations

To distinguish between DNA derived from WT and *Cdkl5*<sup>-/-</sup> male littermates, primers F1, R and F2 were used in the same PCR reaction. Two bands were detected for WT male animals (356 and 135 bp) whereas only one band was detected for *Cdkl5*<sup>-/-</sup> male rats (346 bp) (Fig. 1). To distinguish between DNA derived from WT and heterozygous (*Cdkl5*<sup>+/-</sup>) female littermates, primers F1, R and F3 were used in the same reaction. One band was detected for WT female rats (356 bp) whereas two bands were detected for heterozygous female rats (356 and 129 bp).

Genomic DNA was extracted from fragments of tissue using the HotShot method. PCR was carried out as per the manufacturer's guidelines for GoTaq G2 Polymerase (Promega, M784B) with an annealing temperature of 58 °C and a 1 min extension time. Following initial validation experiments all genotyping was carried out by Transnetyx Inc.

#### Acute slice preparation for electrophysiology

Acute brain slices were prepared from WT and *Cdkl5*<sup>-/-</sup> rats at postnatal day (P) 28 to 35 (unless otherwise noted) similarly to previously described [18]. Briefly, rats were anaesthetised with isoflurane and subsequently decapitated. The brain was rapidly removed and placed in ice-cold carbogenated (95% O<sub>2</sub>/5% CO<sub>2</sub>) sucrose-modified artificial cerebrospinal fluid (in mM: 87 NaCl, 2.5 KCl, 25 NaHCO<sub>3</sub>, 1.25 NaH<sub>2</sub>PO<sub>4</sub>, 25 glucose, 75 sucrose, 7 MgCl<sub>2</sub>, 0.5 CaCl<sub>2</sub>). 400 µm horizontal hippocampal slices were cut on a Vibratome (VT1200s, Leica, Germany). Slices recovered submerged in sucrose-ACSF at 34 °C for 30 min and were then stored at room temperature until needed.

Alternatively, to assess NMDA receptor-mediated EPSCs throughout development and respective pharmacology, P7-22 WT and *Cdkl5*<sup>-/-</sup> rats were rapidly decapitated and the brain removed. Parasagittal slices (400 µm) were prepared on a Leica VT 1200 microtome in ice cold solution containing (in mM) 206 Sucrose, 2.8 KCl, 1.25 NaH<sub>2</sub>PO<sub>4</sub>, 26 NaHCO<sub>3</sub>, 10 Glucose, 10 MgSO<sub>4</sub>, 2 NaAscorbate, 0.4 CaCl<sub>2</sub>, and 2.5 N-acetyl L-cysteine. Scalpel cuts were made to remove CA3 while retaining the CA1 region of the hippocampus with the overlying cortex and dentate gyrus intact for electrophysiology. Slices were then recovered >60 min at room temperature in a submersion chamber in standard artificial cerebral spinal fluid (ACSF), containing (in mM) 124 NaCl, 26 NaHCO<sub>3</sub>, 1.2 NaH<sub>2</sub>PO<sub>4</sub>, 10 D-glucose, 3 KCl, 2 NaAscorbate, 1 MgSO<sub>4</sub>, 2 CaCl<sub>2</sub>, and 2.5 N-acetyl L-cysteine) prior to all experiments. All solutions were oxygenated with 95% O<sub>2</sub> -5% CO<sub>2</sub>.

#### Field LTP recordings

Slices were transferred to a submerged recording chamber perfused with warm carbogenated recording ACSF (in mM: 125 NaCl, 2.5 KCl, 25 NaHCO<sub>3</sub>, 1.25 NaH<sub>2</sub>PO<sub>4</sub>, 25 glucose, 1 MgCl<sub>2</sub>, 2 CaCl<sub>2</sub>) at a flow rate of 3–4 mL/min. Extracellular field recording electrode was filled with recording ACSF and placed in the *stratum radiatum* (*Str Rad*) of the CA1 region. Single pulses of electric stimulation (200 µs, 0.5 Hz) were delivered through a bipolar electrode (Ni: Cr) placed in the *Str Rad* to stimulate the Schaffer collateral (SC) pathway. Stimulus intensity was adjusted to produce 50% of the maximum field excitatory post-synaptic potential (fEPSP) amplitude. LTP was induced by tetanic stimulation (two trains of 1 s 100 Hz stimulation, 20 s inter-train interval [19], following 20 min of stable baseline. fEPSP slopes were normalised to baseline values and LTP magnitude reported as the average fEPSP slope in the final 10 min (50–60 min post-induction) of the recording divided by the average fEPSP slope during the baseline period. Data acquisition and analysis were performed on WinLTP [20].

#### Whole-cell patch-clamp recordings

For whole-cell recordings, slices were transferred to a submerged recording chamber perfused with warm carbogenated recording ACSF (in mM: 125 NaCl, 2.5 KCl, 25 NaHCO<sub>3</sub>, 1.25 NaH<sub>2</sub>PO<sub>4</sub>, 25 glucose, 1 MgCl<sub>2</sub>, 2 CaCl<sub>2</sub>), at a flow rate of 6–8 mL/min. All recordings were performed at 31±1 °C unless otherwise stated. Infrared differential interference contrast (IR-DIC) video microscopy, using a digital camera (Qimaging) mounted on an upright microscope (Olympus BX51WI) and a 40×(0.8NA) water immersion objective was used for all experiments. Recordings were obtained with a Multi-clamp 700B (Molecular Devices) amplifier, signals were Bessel filtered online at 5 kHz and digitized at 20 kHz (Digidata1440, Molecular Devices) coupled to the Clampex software (pCLAMP™ Software, Molecular Devices). Recording pipettes were pulled from borosilicate glass capillaries (1.7 mm outer/1 mm inner diameter, Harvard Apparatus, UK) on a horizontal electrode puller (P-97, Sutter Instruments, CA, USA), with resistance of 4–9 MΩ when filled with internal solution. For voltage-clamp recordings glass electrodes were filled with cesium based internal solution (in mM: 110 CsOH, 110 D-gluconic acid, 20 CsCl, 10 HEPES, 10 phospho-creatine, 4 MgATP, 4 NaCl, 0.3 Na<sub>2</sub>GTP, 0.2 EGTA, 5 QX314Cl) unless stated otherwise. A potassium gluconate based internal solution (in mM 120 K-gluconate, 20 KCl, 10 HEPES, 10 phospho-creatine, 4 MgATP, 4 NaCl, 0.3 Na<sub>2</sub>GTP, 2.7 biocytin, pH=7.4, Osm=290–310) was used for whole-cell current-clamp recordings. Cells were rejected if series resistance >30 MΩ, or the series resistance changed by more than 20% over the course of the recording. No series

resistance cancellation or junction potential corrections were performed.

#### **Evoked EPSCs**

CA3 inputs to CA1 PCs were stimulated by placing a stimulating bipolar electrode (Ni: Cr or insulated tungsten) in the *Str rad* in hippocampal slices with the CA3 containing portion of the slice severed. A single 100  $\mu$ s current pulse was delivered by an isolated constant current simulator (DS3, Digitimer.Ltd or WPI, Sarasota, FL). Evoked EPSCs were recorded in voltage-clamp using a cesium based intracellular solution.

#### **NMDAR/AMPA and paired-pulse ratio**

AMPA receptor-mediated EPSCs were recorded at -70 mV in the presence of 50  $\mu$ M picrotoxin to block GABA<sub>A</sub> receptors. The same cell was then held at +40 mV to record pharmacologically isolated NMDA receptor-mediated EPSCs in the presence of 50  $\mu$ M picrotoxin and 10  $\mu$ M CNQX. NMDAR/AMPA ratios were calculated from peak amplitude of NMDA receptor and AMPA receptor-mediated EPSCs. We assessed paired-pulse ratio by evoking two EPSCs 50 ms apart, whilst holding the cell at -70 mV in the presence of 50  $\mu$ M picrotoxin and calculating the ratio of the amplitude of the second EPSC relative to the first EPSC.

#### **NMDA receptor subunit expression development and pharmacology**

A cesium based internal solution containing (in mM) 135 CsMeSO<sub>4</sub>, 10 HEPES, 10 BAPTA, 5 Qx314, 0.3 NaGTP, 4 Na<sub>2</sub>ATP, 4 MgCl<sub>2</sub>, and 0.1 spermine, pH 7.25 with 1 M CsOH was used. Recordings were performed at room temperature and extracellular solution was exchanged at a flow rate of 3–4 mL/min. AMPA receptor-mediated EPSCs were recorded at -70 mV, and NMDA receptor-mediated EPSCs were recorded at +40 mV. Peak current for NMDA receptor-mediated EPSCs was taken at 70 ms after the peak of the AMPA receptor-mediated EPSC. NMDA receptor sensitivity to block by GluN2B receptor antagonist Ro 25-6981 was determined by recording a 5 min baseline, followed by Ro 25-6981 (5  $\mu$ M) perfusion onto the slice for 20 min.

#### **AMPA-R I-V relationship**

To assess the presence of CP-AMPA receptors, AMPA receptor-mediated EPSCs were recorded in the presence of 50  $\mu$ M picrotoxin to block GABA<sub>A</sub> receptors and 50  $\mu$ M AP-5 to block NMDA receptors, over a range of voltages from -80 mV to +40 mV. Rectification index was calculated by determining the difference of peak EPSC amplitude at -80mV and at +40 mV to EPSC amplitude at 0 mV and calculating the ratio between those two values in order to account for variations in AMPAR reversal

potential across recordings [21]; in this instance, a rectification index of 2 would indicate the absence of rectification. The same intracellular cesium based intracellular solution was used with added 0.1 mM spermine to maintain rectification of GluA2-lacking AMPA receptors.

#### **Minimal stimulation**

Minimal stimulation protocol was used to assess the presence of silent synapses. Once a reliable EPSC was identified at -70mV, stimulus amplitude was reduced until the synaptic response would fail in some of the trials, allowing for the stimulation of a single or a small number of synapses. Following recording of 50 trials at a holding potential of -70 mV, corresponding to AMPA receptor-mediated EPSCs, the cell was depolarised to +40 mV, to reveal mixed AMPA and NMDA receptor-mediated EPSCs and an additional 50 trials were recorded. To determine response probability the traces for each holding potential were visually inspected and the number of traces with a visible EPSC was divided by the total number of traces for each cell. The ratio of response probability at the two holding potentials was used as an estimate for the relative abundance of silent synapses [22, 23].

#### **Miniature EPSC recordings**

Miniature EPSCs (mEPSCs) were recorded in voltage clamp while holding the cell at -70 mV, using a cesium gluconate based internal solution. Recordings were performed in recording ACSF in the presence of 50  $\mu$ M picrotoxin and 300 nM TTX to block voltage gated sodium channels and consequently action potential firing. Analysis of mEPSC frequencies and amplitudes over two minutes of recording was performed using a template matching algorithm [24] in Stimfit [25]. A similar number of mEPSC events were analysed for each condition – around 500 events, on average, per cell.

#### **Intrinsic physiology**

Passive and active membrane properties were assessed to examine intrinsic excitability as previously described [18]. Passive membrane properties, including membrane time constant and input resistance, were measured from the voltage response to a 500 ms hyperpolarizing 10 pA step. Rheobase current and action potential (AP) firing frequency were determined from a series of depolarising current steps (0 to +400 pA, 500 ms) while holding the cell at -70mV with a bias current. AP properties were determined from the first AP elicited. All analysis of electrophysiological data was performed using the open source software package Stimfit [25], blinded to genotype.

### Synaptosome preparation

WT and *Cdk15*<sup>-/-</sup> rats were killed by exposure to increasing CO<sub>2</sub> and decapitated. The hippocampus from each hemisphere was dissected in ice-cold 1x sucrose-EDTA buffer (0.32 M sucrose, 1 mM EDTA, 5 mM Tris, pH 7.4). The tissue was snap-frozen and stored at -80 °C until used for synaptosome preparation. On the day of preparation, the tissue was quickly thawed at 37 °C and homogenized in ice-cold 1x sucrose/EDTA buffer using 5–6 up-and-down strokes of a pre-chilled Teflon glass with motorized homogenizer [26]. Homogenates were centrifuged at 950 x g for 10 min at 4 °C. The discontinuous (3% uppermost, 10% middle and 23% bottom) Percoll-density gradient was prepared prior to homogenization. The supernatant (S1) was added gently on 3% Percoll-sucrose (Percoll, P1644, Sigma Aldrich, UK) and centrifuged at 47,808 x g for 8 min at 4 °C. The fraction between 23% and 10% was collected and re-suspended in HEPES-Buffered-Krebs (HBK; in mM: 118.5 NaCl, 4.7 KCl, 1.18 MgSO<sub>4</sub>, 10 Glucose, 1 Na<sub>2</sub>HPO<sub>4</sub>, 20 HEPES, pH 7.4 balanced with Trizma) followed by centrifugation at 20,199 x g for 15 min at 4 °C. The pellet containing pure synaptosomes was dissolved in RIPA buffer (phosphatase inhibitor and protease inhibitor added). Protein quantification was performed with MicroBCA Assay kit (Pierce BCA protein estimation kit, 23,225, ThermoFisher Scientific).

### Western blots

Approximately 10 µg of synaptosome protein was separated on a precast gradient gel (NuPAGE 4–12% Bis-Tris Protein Gels, NP0336BOX, Thermo Fisher) and transferred to nitrocellulose membrane (AmershamTM Protran® Western Blotting Membrane, Nitrocellulose, GE10600002, Sigma Aldrich) using Bio-Rad transfer apparatus. Total proteins were stained using reversible protein stain kit (Memcode 24,580, Thermo Fisher Scientific) according to the manufacturer's instructions. After removing the stain, membranes were blocked with 1:1 TBST1X: Odyssey Blocking Buffer (P/N-927-50003, LI-COR Biotech.) for an hour at room temperature, followed by overnight incubation with primary antibodies (CDKL5- 1:1000, #HPA002847, Atlas Antibodies-Sigma Aldrich; NMDAR1-1:1000, #700,685, Thermo Fisher; NMDAR2A-1: 1000, #ab169873, Abcam; NMDAR2B-1:1000, #610,417, BD Biosciences; PSD95- 1:2000, #76,115, Abcam; GluR1- 1:1000, #MAB2263, Millipore; GluR2- 1:1000, #MABN1189, Millipore; RIM1/2– 1:2000, #140,203, SYSY; Munc18-1- 1:2000, #116 011, SYSY; SNAP25- 1:1000, #111 011, SYSY; Synapsin1- 1:1000, #ab64581, Abcam; Synaptophysin- 1:10,000, #ab32127, Abcam; VAMP2- 1: 10,000, #ab3347, Abcam) at 4 °C. Membranes were washed with TBST1x(0.1% Tween 20), and incubated for an hour at room temperature with secondary antibodies (IRDye 800CW Goat anti Rabbit

IgG- 1:10,000, #P/N 925-32211; IRDye 680LT Goat anti Mouse IgG- 1:10,000, #P/N 925-68020, LI-COR Biotechnology). Membranes were washed with TBST1X, dried and digitally scanned using Fc Odyssey Infrared Imaging System, LI-COR, UK Ltd. Odyssey software, Licor Image Studio Lite (LCOR Biosciences) was used to quantify individual bands. Data was normalised to respective total protein and then normalised to WT.

### Sample preparation and mass spectrometry

Purified synaptosomes were lysed in 8 M urea with protease and phosphatase inhibitor cocktail, sonicated for 30 s max amplitude and power on the UP200St sonicator (Hielscher – Ultrasound Technology), and protein quantified by BCA using a Nanodrop 1000. Samples (100 µg) were reduced with 5 mM TCEP for 30 min at RT, and 30 mM Iodoacetamide was added for 30 min at RT in the dark. Samples were diluted to 1 M Urea with 50 mM TEAB pH 8.5, and digested with 2 µg Trypsin overnight at 37 °C, before being desalted using a macro-spin column (Harvard Apparatus) according to manufacturer protocol.

For mass spectrometry analysis, peptides were resuspended in HPLC-grade water containing 2% MeCN and 1% TFA to make a final concentration of 1 µg/µl (based on protein concentration prior to digest). Then, 5 µl of samples were injected for analysis. Peptides were separated using 50 cm Acclaim PepMap 100 analytical column (75 µm ID, 3 µm C18) in conjunction with a PepMap trapping column (100 µm × 2 cm, 5 µm C18) (Thermo Scientific) analysed with Orbitrap Fusion Tribrid mass spectrometer (Thermo-Fisher Scientific). Peptides were loaded on to the column in solvent A (3% MeCN, 0.1% FA in HPLC water). A 218 min gradient was performed with 3% solvent A to 35% solvent B (80% MeCN, 0.08% FA), before increasing solvent B to 90% for 5 min, and re-equilibrating with 3% solvent A for 10 min. Settings for data dependent acquisition were MS1 with 120,000 resolution, scan range 400–1,600, charge state 2–7, AGC target of 400,000 and dynamic exclusion of 50 ms with repeat count 1. Peptide ions were fragmented using HCD (30% collision energy) with a resolution of 30,000, and AGC target of 10,000 with a maximum injection of 40 ms. The whole duty cycle was 3 s, during which the instrument performed “top speed” analysis.

### Proteome quantification

Label-free quantification was performed using MaxQuant (v.1.5.7.4) with the following modifications: fixed modification: carbamidomethyl (C); variable modifications oxidation (M), acetylation (protein N-terminus); label-free quantitation with minimum ratio count 2; maximum five modifications per peptide, and two missed cleavages. Searches were conducted using a *Rattus*

*norvegicus* Uniprot-Trembl database (downloaded 27th July 2017 with 36,078 entries) and a list of common contaminants. Identifications were filtered at a 1% false-discovery rate (FDR). Quantification used only razor and unique peptides with a minimum ratio count of 2. “Re-quantify” was enabled. “Match between runs” was used with alignment time window 20 min and match time window 0.7 min. LFQ intensities were used for data analyses. The mass spectrometry proteomics data have been deposited to the ProteomeXchange Consortium via the PRIDE partner repository (<https://www.ebi.ac.uk/pride/>) with the dataset identifier PXD043246 and can be viewed by reviewers with the following details: **Username:** reviewer\_pxd043246@ebi.ac.uk; **Password:** L0K4DUac.

### Histology

Slices used for electrophysiology experiments were fixed in 4% paraformaldehyde (PFA) overnight and stored in PBS (phosphate buffered saline) at 4 °C until used for histology. Slices were washed in PBS and incubated in PBS with 0.3% triton-X and Alexa488 or Alexa568-conjugated streptavidin (1:500 dilution, Molecular probes, Invitrogen, USA) over night. Slices were then washed in PB and mounted on glass slides using Vectashield Hardset mounting medium (H-1400, Vector Labs).

### Image acquisition and analysis

To reconstruct cells and examine their morphology, multiple Z-stacks were taken in order to capture the entire biocytin-filled cell on an inverted confocal microscope (Axiovert LSM510, Zeiss) under a 20x Plan Neofluar (NA 0.5) objective (Zeiss). The Z-stacks obtained for a given cell were stitched using the 3D stitching plug in FIJI (ImageJ), and the cell was reconstructed using the Simple Neurite Tracer plug-in [27]. Sholl analysis was then performed on the skeletonised paths to examine dendritic complexity. To examine spine distribution in biocytin-filled cells, Z-stacks were taken from basal and apical (oblique and tuft) dendrites (2–3 dendrite sections per dendrite type per cell). Spines were imaged under a 63x Plan Apochromat (NA 1.4) oil immersion objective on an inverted confocal microscope (Axiovert LSM510, Zeiss), with a 2.8x zoom, 2x average line scan, 1024×1024 resolution, 0.14 μm Z step. Huygens Essential software (Scientific volume imaging, Netherlands) was used for deconvolution. The deconvolved images were used for analysis on FIJI (ImageJ). Z-projections of the deconvolved Z-stacks were used to manually count spines using the cell counter tool. For each dendrite section, the number of spines was normalised to the length of the section of dendrite analysed.

### Statistical analysis

All experiments and data analysis were performed blind to genotype. All statistics were performed using linear mixed effects modelling (or the generalised form), when such analysis was not possible data were compared using animal averages to avoid the risk of type-1 statistical errors. Mixed modelling was implemented using the R package lme4 in RStudio [28]. Genotype was set as fixed effect and animal, slice (and cell where relevant) as random effects, allowing for direct measurement of genotype effect while accounting for the variability resulting from random effects. For alternative statistical tests Graphpad prism 7 was used to perform comparisons across groups with two-tailed unpaired T-tests, repeated measures two-way ANOVA, or non-parametric tests as appropriate. In many figures data are shown from both cell and animal, the latter delineated through the use of the prime (′) symbol. Where only one dataset is shown, these are generated from animal averages unless otherwise stated in the figure legend. Details on sample size and statistical test used are presented in the results text and figure legends.

## Results

### Validation of *Cdkl5*<sup>-/-</sup> rats

In collaboration with Horizon Discovery, the *Cdkl5*<sup>-/-</sup> rat model was created using CRISPR/Cas9 technology to introduce a 10 bp (bp) deletion in exon 8 of the *Cdkl5* gene (Ensembl coordinates X:35,674,763–35,674,772, in the Rnor\_6.0 genome assembly). The deletion in constitutive exon 8 of the *Cdkl5* gene leads to a premature stop codon in constitutive exon 9 (Fig. 1A). A genotyping strategy with primers flanking (F1, R) and overlapping (F2) the deletion site was used to distinguish WT and *Cdkl5*<sup>-/-</sup> animals, with two bands detected for WT males (356 and 135 bp) whereas only one band was present for *Cdkl5*<sup>-/-</sup> rats (346 bp) (Fig. 1A–B). Examination of RNA-seq reads mapping to the *Cdkl5* locus confirmed the 10 bp deletion and revealed no cryptic splicing around the deletion. Thus, all transcripts produced from the locus are expected to contain the premature stop codon. The lack of CDKL5 protein expression was confirmed by western blot in hippocampal and prefrontal cortex tissue preparations, where the 115 kDa band corresponding to CDKL5 is present in WT but almost undetectable in *Cdkl5*<sup>-/-</sup> rats (Fig. 1C, quantified in 1D). Furthermore, there was an absence of CDKL5 expression in hippocampal synaptosome preparations from *Cdkl5*<sup>-/-</sup> rats (Fig. 1E, quantified in 1 F) *Cdkl5*<sup>-/-</sup> rats were generally healthy with lighter body weights at four weeks of age (WT=112.5±7.8 g (*n*=10), *Cdkl5*<sup>-/-</sup> = 85.8±6.5 g (*n*=11); *p*=0.0177) but this difference was absent in older animals. *Cdkl5*<sup>-/-</sup> rats did not exhibit observable spontaneous seizures.

**Table 1** Passive membrane properties of CA1 pyramidal cells are unaltered in *Cdk15<sup>-/-</sup>* rats

Physiological property	WT	<i>Cdk15<sup>-/-</sup></i>	<i>p</i> value (LMM)
Resting membrane potential (mV)	-69.8±1.2	-69.2±1.1	0.56
Input resistance (MΩ)	68.1±6.8	65.4±3.0	0.64
Membrane time constant (ms)	19.1±1.0	20.7±2.1	0.64
Capacitance (pF)	299±23	331±35	0.69

***Cdk15<sup>-/-</sup>* CA1 pyramidal cells exhibit typical cellular excitability**

We first examined cellular excitability of *Cdk15<sup>-/-</sup>* CA1 pyramidal cells, as altered cellular excitability has been suggested to contribute to circuit level dysfunction in autism spectrum disorder (ASD)/ID and epilepsy [29, 30]. CA1 PCs from WT rats exhibited a hyperpolarised resting membrane potential, fast membrane time constant and low input resistance (Table 1), in line with previous studies [31, 32]. WT CA1 PCs required 206±20 pA of current injection to elicit the first AP (rheobase, Fig. 2C, C'), and the number of APs fired increased with current injection thereafter until reaching a firing frequency of 22±2 Hz in response to the maximum current injection step (400 pA, Fig. 2A, D, D'). In *Cdk15<sup>-/-</sup>*

rats, passive membrane properties (Table 1; Fig. 2B, B'), rheobase current (LMM, *p*=0.91, Fig. 2C, C') and overall AP firing in response to increasing current steps (Two-Way ANOVA *F* (16, 208)=0.12, genotype effect: *p*=0.66, Fig. 2D, D'), and were unaffected. These data indicate intrinsic neuronal excitability is unaffected in *Cdk15<sup>-/-</sup>* rats.

**Enhanced hippocampal LTP in *Cdk15<sup>-/-</sup>* rats**

To examine synaptic plasticity in the hippocampus of *Cdk15<sup>-/-</sup>* rats, we performed extracellular field recordings in horizontal hippocampal slices from *Cdk15<sup>-/-</sup>* rats and their WT littermate controls aged P28 to P35. We measured the slope of the field EPSP evoked by stimulation of Schaffer collateral inputs to CA1 over a baseline period of 20 min and for 1 h following tetanic stimulation (Fig. 3). Analysis of the LTP time course (Fig. 3B) and the EPSP slope in the final 10 min of the recording as a percentage of the baseline EPSP slope (Fig. 3C) revealed an enhanced LTP in *Cdk15<sup>-/-</sup>* rats (176.1±5.6%) relative to WT (138.3±5.8%, Two tailed T test, *T*=4.45, *df*=19, *p*=0.003). Interestingly, this is a transient effect as the magnitude of LTP is restored to WT levels by 12 weeks of age (Supplemental Fig. 1).

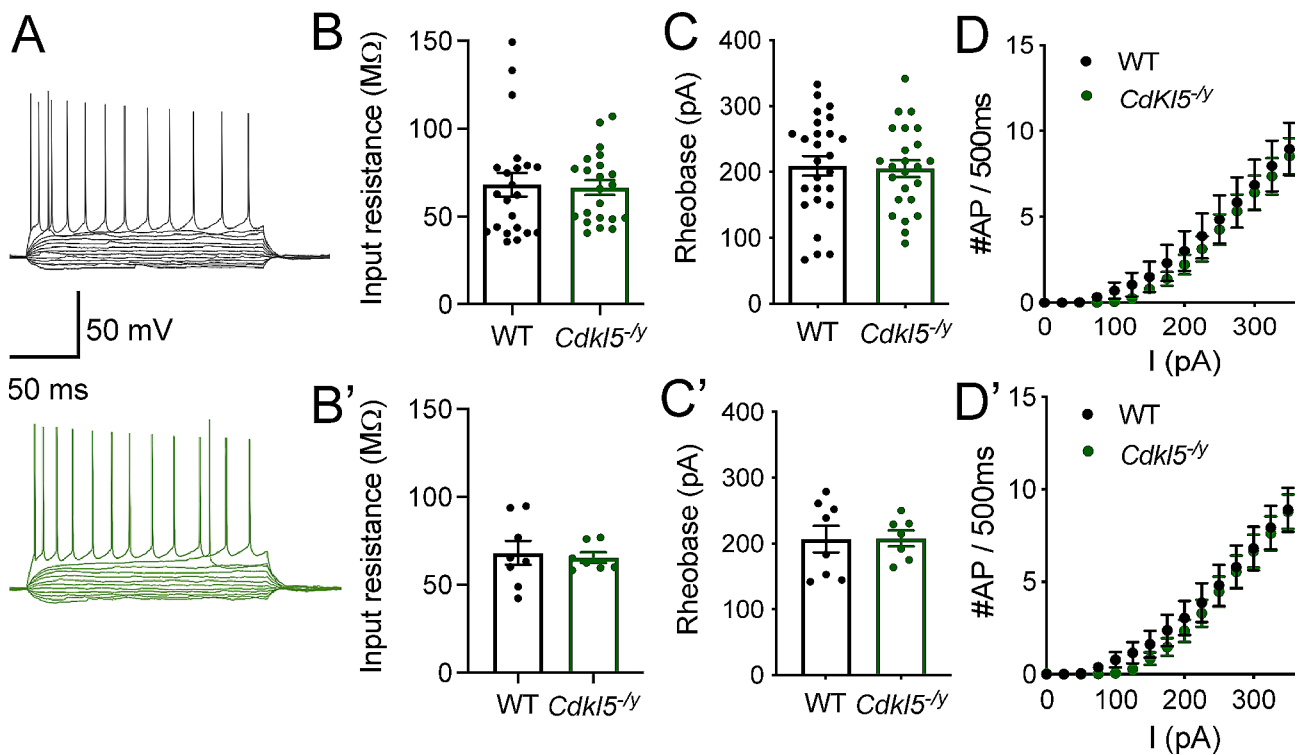


**Fig. 2** Typical excitability of CA1 pyramidal cells. **(A)** Representative traces of whole cell recordings from WT (black, upper) and *Cdk15<sup>-/-</sup>* (green, lower) CA1 pyramidal cells in response to subsequent 25 pA steps. Traces shown from -100 pA to rheobase-1 and for the maximum firing frequency (*I* = 400 pA). **(B, B')** Input resistance. **(C, C')** rheobase current. **(D, D')** Action potential discharge in response to 500 ms long 25 pA current steps up to 400 pA (Two-way ANOVA genotype effect *F*<sub>16,208</sub>=0.12, *p*=0.66). Data shown as mean ± SEM (WT - *n*=26 cells/8 rats, *Cdk15<sup>-/-</sup>* - *n*=24 cells/7 rats, data points represent single cells **(B, C, D)** or animal averages **(B', C', D')**)

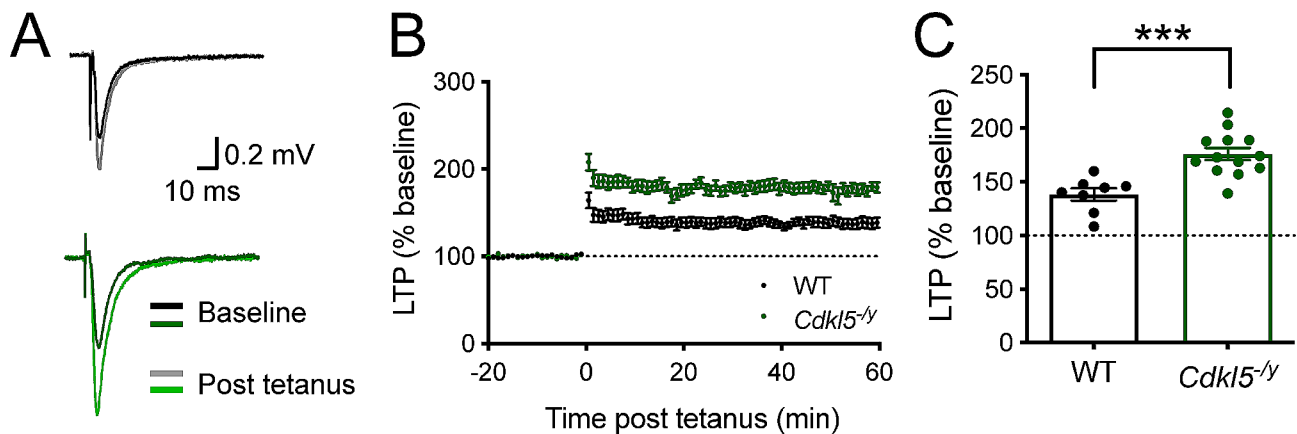


**Fig. 3** Hippocampal long term potentiation (LTP) in juvenile *Cdkl5*<sup>-/-</sup> rats. **(A)** Representative WT (upper) and *Cdkl5*<sup>-/-</sup> (lower) fEPSP traces before (baseline) and after (post tetanus) LTP induction. **(B)** Time-course showing long term potentiation (LTP) in the hippocampal CA1 induced by two trains with 100 pulses at 100 Hz (20 s apart), resulting in a significant increase in LTP in *Cdkl5*<sup>-/-</sup> rats when compared to WT. **(C)** LTP in the final 10 min of the recording relative to baseline (WT *n*=8 rats; *Cdkl5*<sup>-/-</sup>: *n*=13 rats; \**p*<0.05 Two tailed T test, data points represent animal averages)

#### Unaltered NMDA receptor and AMPA receptor function

Both AMPA receptor and NMDA receptor dysfunction and altered subunit composition have been implicated in abnormal LTP in mouse models of CDD [12, 13]. We assessed the NMDAR/AMPA ratios of synaptic responses at the SC synapse of CA1, to test whether NMDA receptor function was altered in *Cdkl5*<sup>-/-</sup> rats, possibly contributing to the enhanced LTP phenotype observed. AMPA receptor-mediated currents were recorded at a holding potential of -70 mV, whilst NMDA receptor-mediated EPSCs were recorded at +40 mV in the presence of the AMPA receptor antagonist CNQX (Fig. 4A). CA1 pyramidal neurons in WT rats exhibited NMDAR/AMPA ratio of  $0.62 \pm 0.08$  (Fig. 4B, B') and an average NMDA receptor-mediated EPSC decay time of  $85.69 \pm 5.07$  ms (Fig. 4C, C'), which were unaltered in *Cdkl5*<sup>-/-</sup> rats ( $0.84 \pm 0.14$ , GLMM: *p*=0.31;  $105.3 \pm 16.50$  ms, *p*=0.78 Mann-Whitney test, respectively). These data indicate NMDA receptor function and subunit composition is unaltered in the absence of CDKL5. In line with the findings from electrophysiology experiments, the expression of NMDA receptor subunits GluN1, GluN2A and GluN2B was unaffected in the absence of CDKL5, as seen by comparable expression levels of these proteins in hippocampal synaptosome preparations from WT and *Cdkl5*<sup>-/-</sup> rats (Fig. 4D-G).

Nonetheless, NMDA receptor subunit composition undergoes a developmental switch and has an important role in regulating AMPA receptor presence at synapses [17]. To the best of our knowledge, NMDA receptor subunit expression development has not yet been studied in preclinical models of CDD, as studies conducted in mouse models have been largely restricted to adults. As such we examined NMDA receptor function over development to assess whether the developmental trajectory of NMDA receptor subunit composition is altered

in *Cdkl5*<sup>-/-</sup> rats, potentially contributing to long lasting effects at the circuit level.

NMDAR/AMPA ratios and decay time constant of NMDA receptor-mediated EPSC were assessed in CA1 PCs from P7-22 rats (Fig. 5A, B). In WT rats, the NMDAR/AMPA ratio decreased from  $1.24 \pm 0.27$  at P7-11 to  $0.54 \pm 0.13$  at P18-22 (Figs. 2 and 5A-Way ANOVA age effect: *F* (2, 36)=5.821, *p*=0.006), consistent with increased expression of AMPA receptor as development progresses [33]. This was accompanied by a reduction in decay time constant of the NMDA receptor-mediated EPSC from  $562.9 \pm 43.4$  ms to  $245.2 \pm 20.3$  ms over the same period (Figs. 2 and 5B-Way ANOVA age effect: *F* (2, 36)=25.77, *p*<0.0001), consistent with an increased contribution of the NMDA receptor subunit GluN2A to synaptic transmission during development [34].

*Cdkl5*<sup>-/-</sup> rats followed a similar developmental trajectory with NMDAR/AMPA decreasing from  $1.12 \pm 0.32$  to  $0.46 \pm 0.06$ , and decay time from  $534.4 \pm 73.12$  ms to  $294.0 \pm 16.9$  ms. This was not significantly different from WT when tested with a 2-way ANOVA performed on animal averages (NMDAR/AMPA - Interaction: *F* (2, 36)=0.1397, *p*=0.87, genotype effect: *F* (1, 36)=0.1043, *p*=0.75; decay time - interaction: *F* (2, 36)=0.5142, *p*=0.60, genotype effect: *F* (1, 36)=0.2326, *p*=0.63). Recordings in the presence of the GluN2B receptor antagonist Ro 25-6981 were performed to further examine the subunit composition of NMDA receptors during development (Fig. 5C-E). The percentage of NMDA receptor-mediated current blocked in the presence of Ro 25-6981 decreased with age from  $65.99 \pm 6.18\%$  at P7-11 to  $48.06 \pm 8.80\%$  at P18-22 in WT rats. The block produced by Ro 25-6981 application was unaltered in *Cdkl5*<sup>-/-</sup> rats (Fig. 5E, Two-Way ANOVA Interaction: *F* (2, 26)=0.542, *p*=0.59, genotype effect: *F* (1, 26)=0.002,

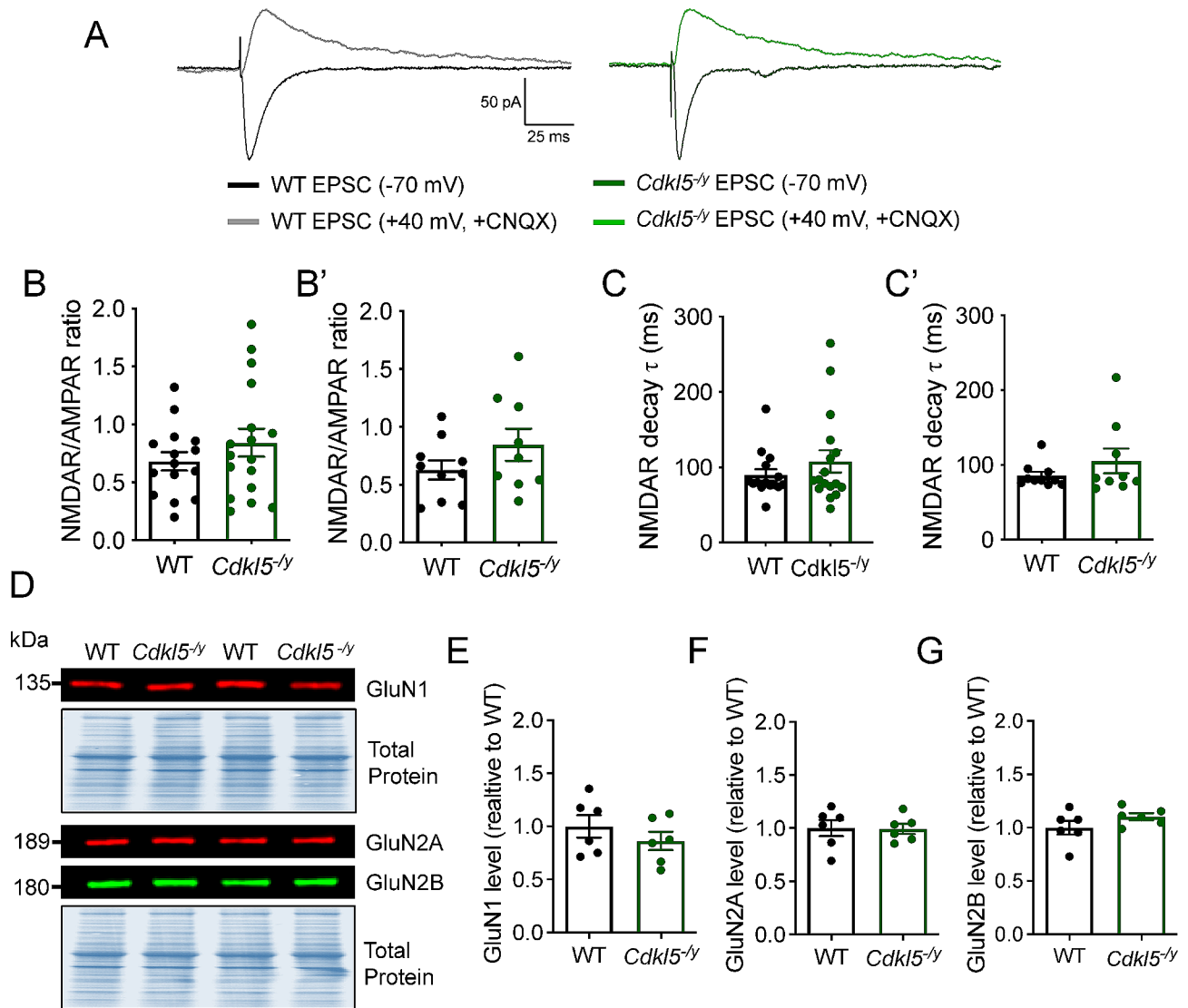


**Fig. 4** Unaltered NMDA receptor function and subunit composition in the hippocampus of P28-35 *Cdk15*<sup>-/-</sup> rats. **(A)** Representative traces of AMPA receptor and NMDA receptor-mediated currents evoked by stimulating Schaffer collateral inputs to CA1. **(B, B')** NMDAR/AMPA ratio ( $p=0.31$  GLMM), **(C, C')** Pharmacologically isolated NMDA receptor-mediated EPSC decay time ( $p=0.78$  Mann-Whitney U test performed on animal averages). Data shown as mean  $\pm$  SEM (WT  $n=10$  rats / 14 cells; *Cdk15*<sup>-/-</sup>:  $n=9$  rats / 18 cells), data points represent individual cells **(B, C)** and respective animal averages **(B', C')**. **(D)** Representative western blot images from synaptosome preparations probed for NMDA receptor subunits GluN1, GluN2A, GluN2B and respective Total Protein stain. **(E–G)** Quantification of protein expression level normalised to total protein and WT. Data shown as mean  $\pm$  SEM. ns- $p > 0.05$  Two-tailed T test

$p=0.97$ ). These data are further supported by the similar expression of NMDA receptor subunits in synaptosome preparations across genotypes in P14 rats (Supplemental Figure S2). Overall, these data suggest that the developmental switch in NMDA receptor subunit composition and NMDA receptor contribution to synaptic transmission is unaltered in *Cdk15*<sup>-/-</sup> rats.

In addition to NMDA receptors, altered AMPA receptor subunit composition has been suggested as a potential mechanism underlying enhanced early-phase LTP in mouse models of CDD, where higher levels of CP GluA2-lacking AMPA receptors were observed at baseline [13]. To assess the relative abundance of CP-AMPA receptors,

we recorded AMPA receptor-mediated EPSCs by stimulating the SC inputs to CA1 and performing whole cell voltage clamp recordings from CA1 PCs in the presence of NMDA receptor and GABA<sub>A</sub> receptor blockers (Fig. 6). AMPA receptor-mediated EPSCs were recorded at a range of voltages from  $-80$  mV to  $+40$  mV in order to assess their current-voltage (I-V) relationship and rectification index. To maintain the intracellular polyamine block that confers inward rectification characteristic of CP-AMPA receptors, the intracellular solution in the recording pipette contained 0.1 mM of spermine [35].

AMPA receptor-mediated EPSCs exhibited a linear current-voltage I-V relationship in WT neurons (Fig. 6B,

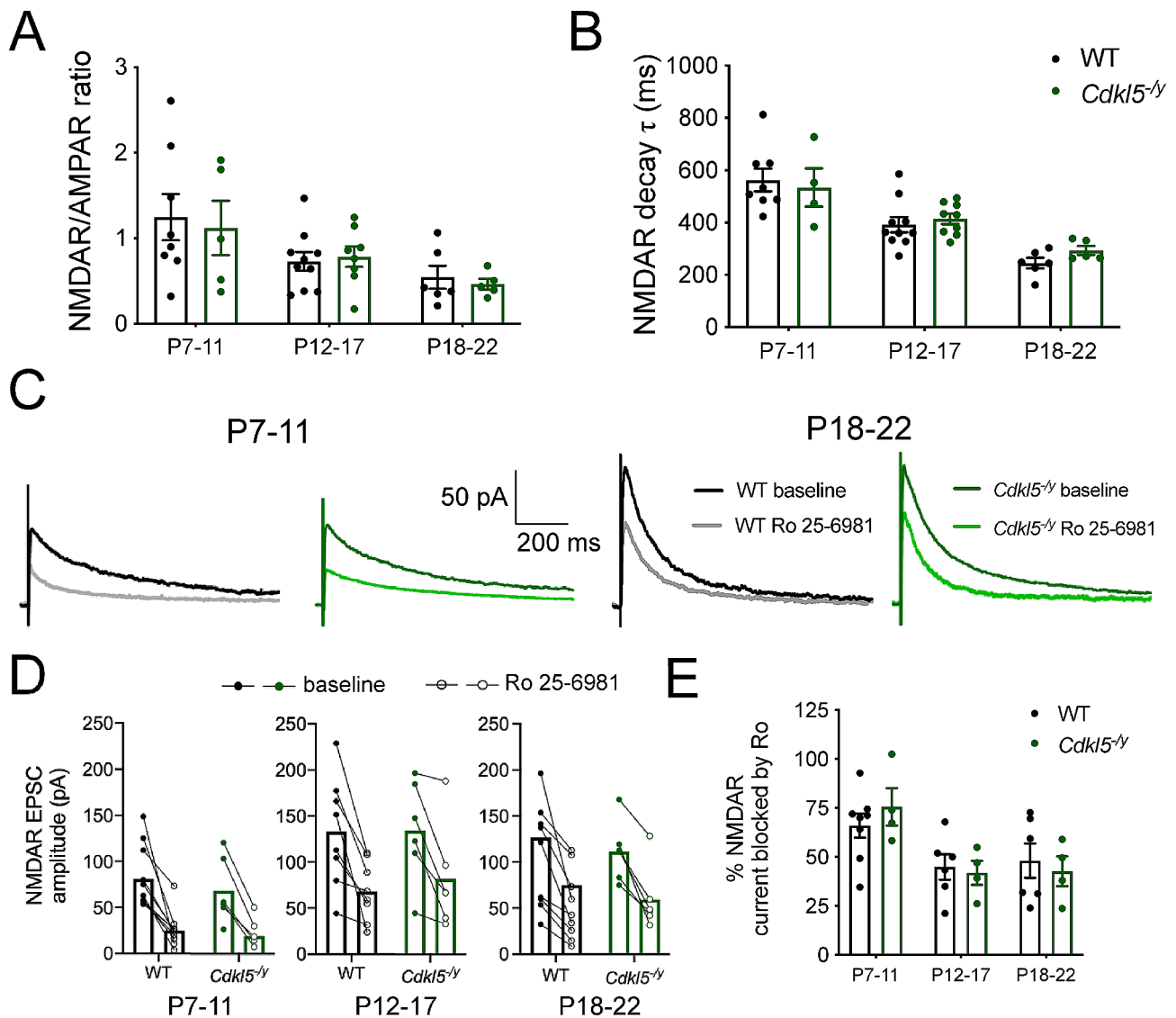


**Fig. 5** Typical NMDA receptor developmental trajectory in *Cdkl5*<sup>-/-</sup> rats. **(A)** NMDAR/AMPA ratio in WT and *Cdkl5*<sup>-/-</sup> rats aged P7 to P22. **(B)** NMDAR decay time constant over development. **(C)** Representative traces of NMDA receptor-mediated EPSCs in the presence or absence (baseline) of the GluN2B antagonist Ro 25-6981. **(D)** NMDA receptor-mediated EPSC amplitude for individual cells before (full circles) and after (clear circles) Ro 25-6981 application, with recordings from each cell connected by a straight line across 3 age groups examined. **(E)** Percentage of NMDA receptor current blocked by RO 25-6981 based on cells shown in **(D)**. All data shown as mean  $\pm$  SEM, data points represent animal averages (except in **D**)

B'), indicating no inward rectification and consistent with the high GluA2 expression in CA1 PCs [33, 36] In *Cdkl5*<sup>-/-</sup> rats this linear relationship was maintained and did not differ to that observed in WT rats (Fig. 6B, B';  $F(1,143)=2.3$ ,  $p=0.13$ , Sum-of-least squares F-test). To test whether there was a difference in reversal potential between genotypes, we fitted the individual I/Vs for each recording to obtain a mean reversal potential for WT and *Cdkl5*<sup>-/-</sup> CA1 neurons. The mean reversal potentials were not significantly different between genotypes (WT:  $5.93 \pm 2.04$  mV, *Cdkl5*<sup>-/-</sup>:  $1.67 \pm 2.87$  mV;  $T=1.19$ ,  $df=19$ ,  $p=0.25$ , Two Tailed T test).

The rectification index, obtained by subtracting EPSC amplitude at 0 mV from EPSC amplitude at the holding potentials of -80 mV and +40 mV and dividing these two values, was also unchanged in the absence of CDKL5 (Fig. 6C, C'; WT:  $2.13 \pm 0.13$ , *Cdkl5*<sup>-/-</sup>:  $1.98 \pm 0.17$ ,  $p=0.32$  LMM). Using our method, a rectification index of 2 indicates the absence of rectification. Together these data suggest that NMDA receptor and AMPA receptor-mediated synaptic transmission are not affected in *Cdkl5*<sup>-/-</sup> rats and therefore alterations to NMDA receptor and AMPA receptor populations are unlikely to contribute to the enhanced LTP observed in the rat model of CDD.

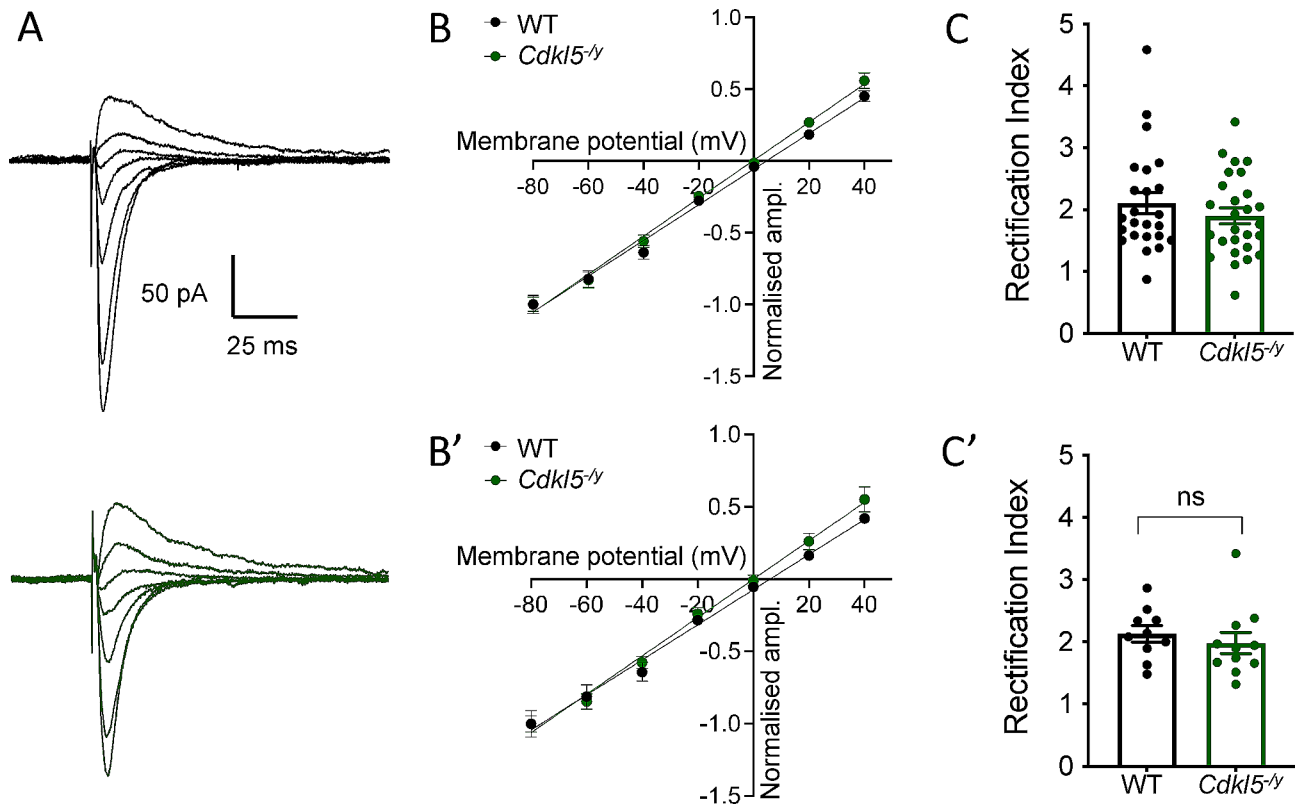


**Fig. 6** Unaltered AMPA receptor-mediated EPSC I-V relationship in CA1 pyramidal cells of *Cdkl5*<sup>-/-</sup> rats. **(A)** Representative traces of AMPA receptor-mediated currents from WT (upper, black) and *Cdkl5*<sup>-/-</sup> (lower, green) recorded over a range of holding potentials (-80mV to +40 mV) in the presence of 0.1mM spermine in the intracellular solution. **(B, B')** I-V relationship AMPA receptor-mediated EPSC normalised to EPSC amplitude at -80 mV holding potential (Genotype effect:  $F_{1,11}=1.794$ ,  $p=0.21$ , Two-way ANOVA) **(C)** Rectification index calculated as the ratio of the difference EPSC amplitude between 0 mV and -80 mV and 0 mV and +40 mV. Data shown as mean  $\pm$  SEM, data shown for individual cells **(B, C)** and animal averages **(B', C')** (WT  $n=24$  cells / 10 rats; *Cdkl5*<sup>-/-</sup>:  $n=27$  cells / 11 rats)

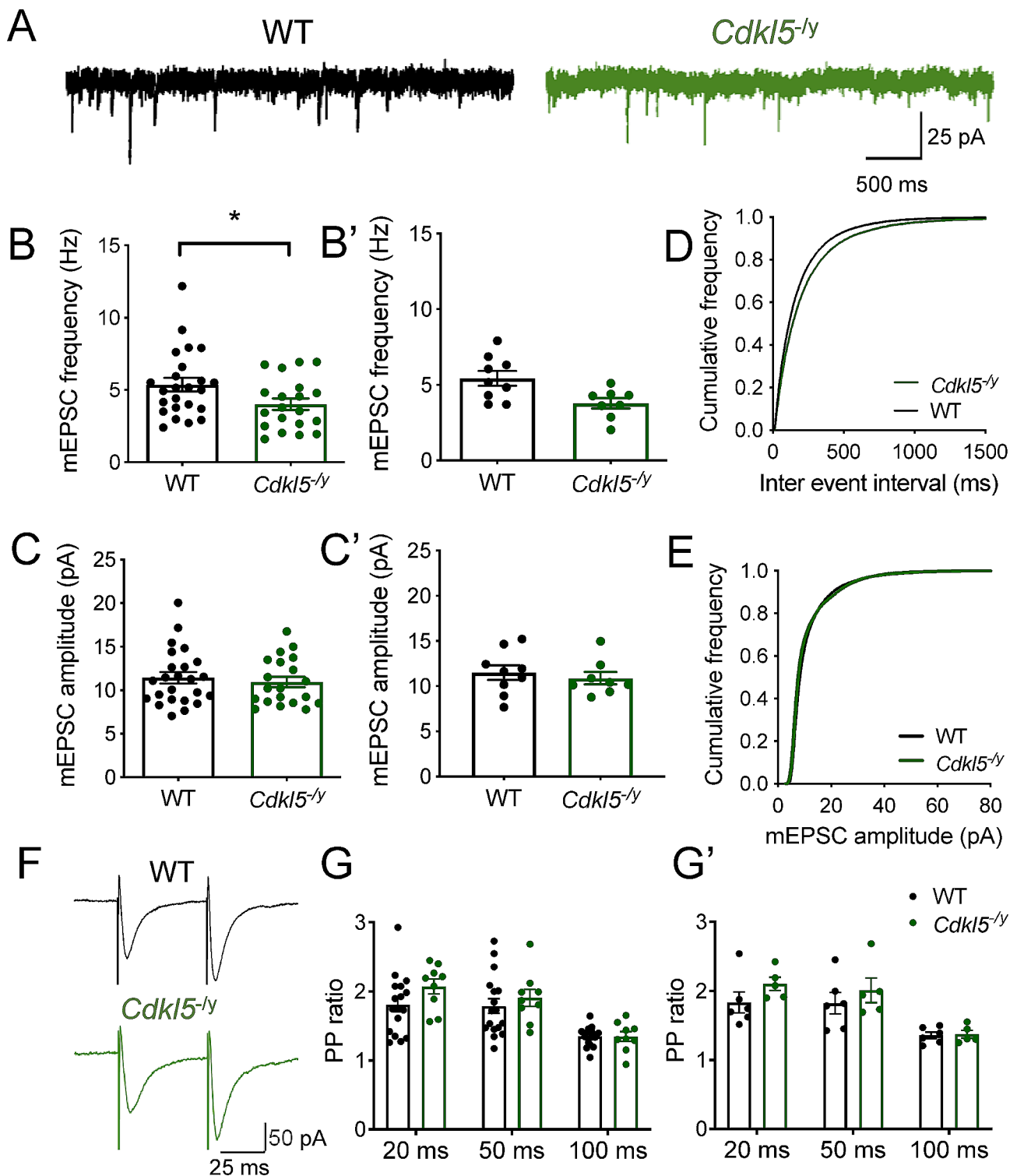
### Reduced mEPSC frequency and unaltered paired-pulse ratio in *Cdkl5*<sup>-/-</sup> rats

In addition to post-synaptic mechanisms mediated by NMDA receptors and AMPA receptors, altered pre-synaptic function can contribute to abnormal synaptic transmission and altered synaptic plasticity. Indeed, CDKL5 function has been implicated at the pre-synapse including through phosphorylation of the pre-synaptic protein amphiphysin-1 [37] and through its interaction with shootin1, which is thought to underlie normal axon specification [38]. Moreover, reduced expression of the pre-synaptic marker synaptophysin has been reported in cellular models of CDD [39, 40]. To assess further synaptic transmission in the absence of CDKL5, we recorded mEPSCs (Fig. 7) and found a 30% reduction in mEPSC frequency from  $5.43 \pm 0.49$  Hz in WT to  $3.78 \pm 0.34$  Hz in *Cdkl5*<sup>-/-</sup> rats (Fig. 7B, B'; LMM  $p=0.02$ ). This was accompanied by unaltered mEPSC amplitudes (Fig. 7C, C'; WT:  $11.51 \pm 0.82$  pA, *Cdkl5*<sup>-/-</sup>:  $10.88 \pm 0.69$  pA, LMM  $p=0.64$ ).

Paired-pulse ratio (PPR) measurements can be used to assess presynaptic release probability [41], thus we examined PPR of evoked EPSCs in response to multiple

stimulus intervals to determine whether the reduction in mEPSC frequency observed was a consequence of reduced pre-synaptic release probability. In WT rats, 2 pulses of electrical stimulation of SC inputs were delivered to CA1 either 20, 50 or 100 ms apart, which resulted in a facilitating postsynaptic response with PPRs of  $1.81 \pm 0.11$ ,  $1.79 \pm 0.11$ , and  $1.35 \pm 0.04$ , respectively. In *Cdkl5*<sup>-/-</sup> rats, EPSCs exhibited a PPR of  $2.07 \pm 0.12$ ,  $1.91 \pm 0.13$ , and  $1.35 \pm 0.08$  in response to the same inter-stimulus intervals (Fig. 7G, G'). There was no statistical difference between genotypes at any tested stimulus interval (Two-way ANOVA of animal averages, Interaction:  $F_{1,9}=1.163$ ,  $p=0.31$  for genotype). Consistent with this, we also found no change in the expression of pre-synaptic markers in *Cdkl5*<sup>-/-</sup> rats (Supplemental Fig. 3).

To determine more global changes in synaptic protein expression, label-free, quantitative mass spectrometry was performed on nerve terminals isolated from P14 hippocampus of either *Cdkl5*<sup>-/-</sup> rats or WT littermate controls. A total of 4356 proteins were identified, with 17 proteins significantly increased in *Cdkl5*<sup>-/-</sup> nerve terminals and 26 significantly decreased (Additional File



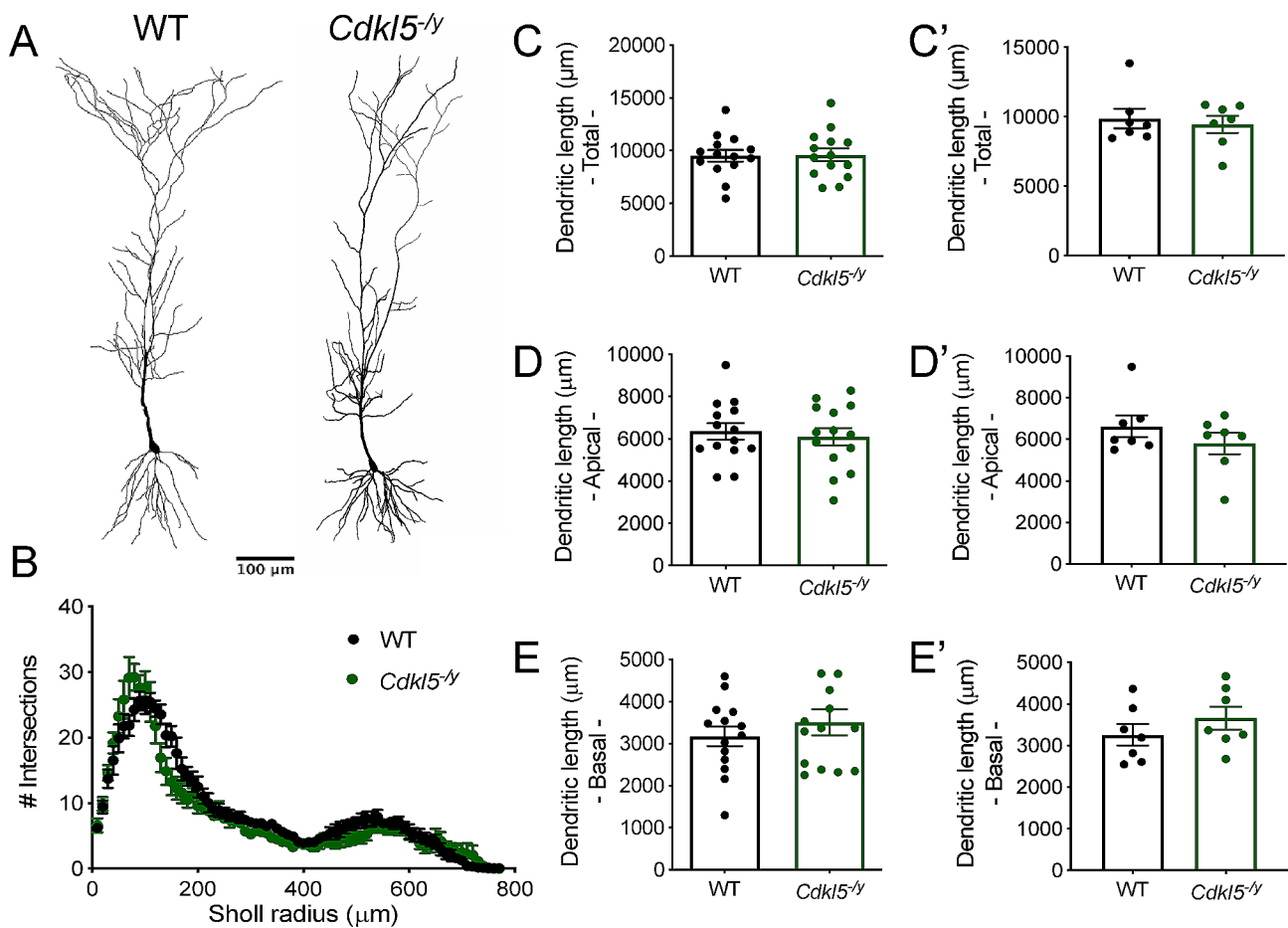
**Fig. 7** Reduced mEPSC frequency and typical PPR in CA1 pyramidal cells from *Cdk15<sup>-/-</sup>* rats. **(A)** Representative traces of mEPSC recordings from WT (left, black) and *Cdk15<sup>-/-</sup>* (right, green) rats. **(B–B')** mEPSC frequency. **(C–C')** mEPSC amplitude: WT  $n=24$  cells / 9 rats, *Cdk15<sup>-/-</sup>*  $n=20$  cells / 8 rats. **(D)** Cumulative distribution of inter-event interval. **(E)** Cumulative distribution of mEPSC amplitude. **(F)** Representative traces of EPSCs evoked by PP stimulation of Schaffer collateral inputs to CA1 pyramidal cells from WT (upper, black) and *Cdk15<sup>-/-</sup>* rats (lower, green) at an interstimulus interval of 50 ms. **(G)** PPR of evoked (WT  $n=18$  cells / 7 rats, *Cdk15<sup>-/-</sup>*  $n=9$  cells / 5 rats) at paired-pulse intervals of 20, 50 and 100 ms. Data in bar charts shown as mean  $\pm$  SEM (data points represent individual cells **(B, C, G)** or corresponding animal averages **(B', C', G')**)

Table 1). Importantly, no CDKL5 peptides were detected in any sample from *Cdkl5*<sup>-/-</sup> rats, confirming our Western blot analysis (Fig. 1). The number of significantly altered proteins in *Cdkl5*<sup>-/-</sup> synaptosomes was relatively small, with only 3 demonstrating a two-fold change (equivalent to 1 on a log2 scale, Additional File Table 1) compared to WT controls. Because of this, *in silico* analysis of convergent molecular pathways was not able to be performed. Significantly upregulated proteins in *Cdkl5*<sup>-/-</sup> synaptosomes included Kv channel-interacting protein 4 (Kcni4), an auxiliary Kv channel subunit reported to favour the open state of these channels [42, 43] and the long isoform of the GABA<sub>A</sub> receptor  $\gamma$ 2 subunit (Gabrg2), suggesting compensatory alterations to hyperexcitability.

**Typical dendritic morphology but increased spine density in basal dendrites of CA1 pyramidal cells**

Altered dendritic morphology has previously been reported in mouse models of CDD across multiple

brain areas [10, 11, 15]. Moreover, dendritic morphology can have a profound impact on processing of synaptic inputs and consequently on circuit level function [44, 45]. As such, we reconstructed biocytin-filled cells in order to examine dendritic arborisation and spine density in *Cdkl5*<sup>-/-</sup> rats (Figs. 8 and 9). In WT rats, biocytin-filled cells exhibited typical CA1 PC morphology (Fig. 8A [46, 47]), . When examining the Sholl profile we found cell morphology to be minimally altered in *Cdkl5*<sup>-/-</sup> rats relative to WT controls (Fig. 8B, Two-way ANOVA of animal averages, Interaction:  $F_{1,12} = 0.822$ ,  $p = 0.38$  for genotype). However, there was a difference in the interaction between Sholl intersections and genotype (two-way ANOVA of animal averages, Interaction:  $F_{76,912} = 2.094$ ,  $p < 0.001$ ), which was predominantly in the proximal (<200  $\mu$ m) dendritic domain. However, the dendritic length (Fig. 8C, C'; WT:  $9882 \pm 707 \mu$ m, *Cdkl5*<sup>-/-</sup>:  $9455 \pm 610 \mu$ m, Two-tailed T Test:  $T_{12} = 0.46$ ,  $p = 0.66$ ) as well as total length of apical (Fig. 8D, D' WT:



**Fig. 8** CA1 pyramidal cell morphology and spine density across multiple dendritic compartments. (A) Example reconstruction of CA1 pyramidal cells from WT and *Cdkl5*<sup>-/-</sup> rats filled with biocytin during whole cell patch clamp recordings. (B) Sholl analysis of the dendritic arborisation (Two way ANOVA: Interaction:  $F_{76,912} = 2.094$ ,  $p < 0.001$ , genotype effect  $p = 0.38$ ). (C) Total dendritic length, (D) total length of basal dendrites, (E) total length of apical dendrites. Data shown as mean  $\pm$  SEM (WT -  $n = 14$  cells/7 rats, *Cdkl5*<sup>-/-</sup> -  $n = 14$  cells/7 rats, data points represent animal averages, all  $p$  values  $> 0.05$ , Two tailed t-test)

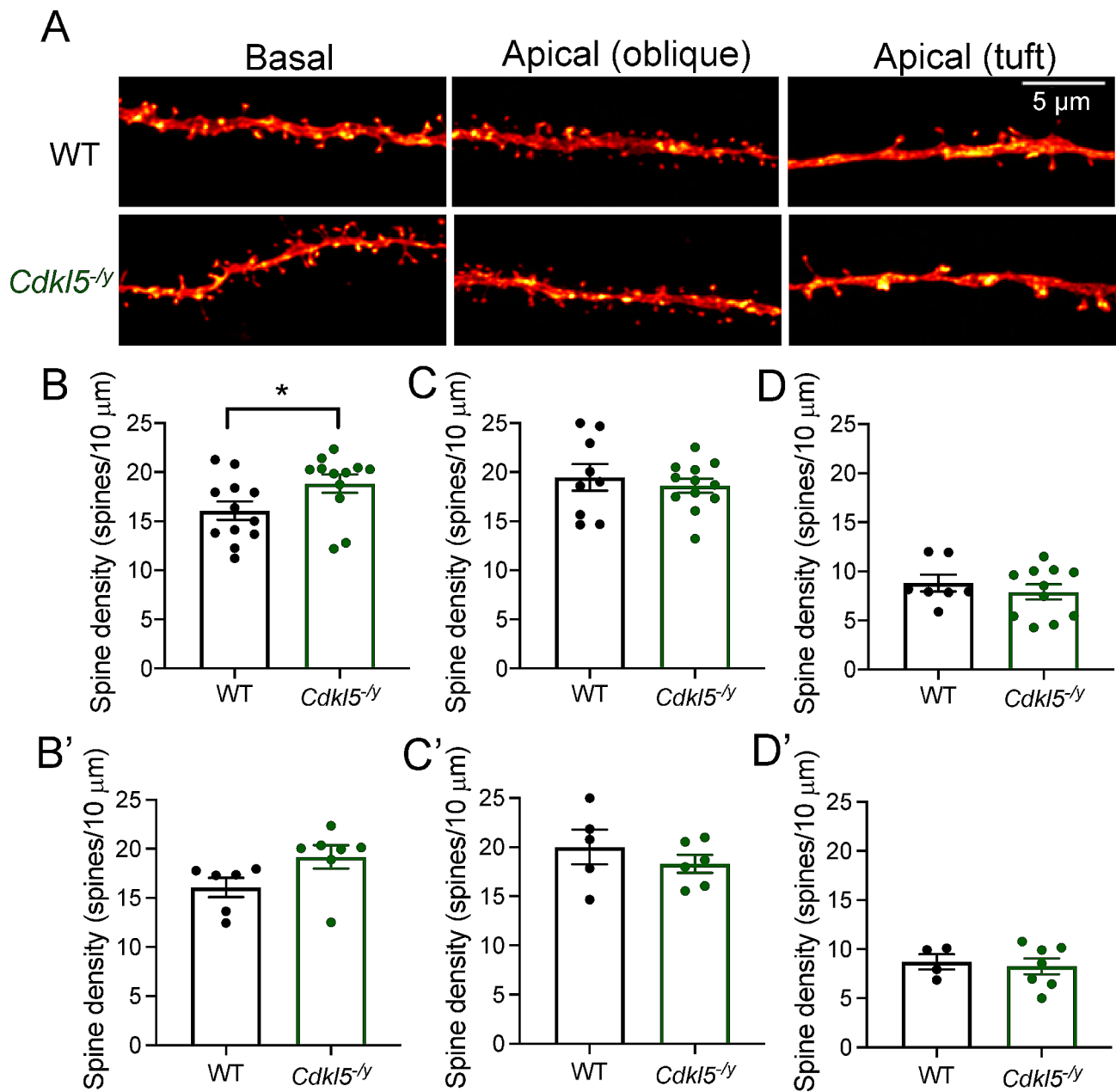


**Fig. 9** Spine density across dendritic compartments of CA1 pyramidal cells. **(A)** Representative segments of basal and apical (oblique and tuft) dendrites from CA1 pyramidal cells filled during whole-cell patch-clamp recordings. **(B)** Spine density in basal dendrites (WT: n = 12 cells/6 rats, *Cdkl5*<sup>-/-</sup>: n = 12 cells / 7 rats). **(C)** Spine density in apical oblique dendrites (WT: n = 9 cells / 6 rats, *Cdkl5*<sup>-/-</sup>: n = 12 cells / 6 rats). **(D)** Spine density in apical tuft dendrites (WT: n = 7 cells/4 rats, *Cdkl5*<sup>-/-</sup>: n = 11 cells / 7 rats). Data shown as mean ± SEM, data points represent cell **(B, C, D)** or animal averages **(B', C', D')**. \**p* < 0.05, ns *p* > 0.05 LMM

6622 ± 520 μm, *Cdkl5*<sup>-/-</sup>: 5795 ± 519 μm, Two-tailed T Test:  $T_{12} = 1.12$ , *p* = 0.28) and basal dendrites (Fig. 8E, E'; WT: 3260 ± 257 μm, *Cdkl5*<sup>-/-</sup>: 3660 ± 275 μm, Two-tailed T Test:  $T_{12} = 1.06$ , *p* = 0.31) were unchanged, indicating that overall dendritic complexity is minimally affected by the lack of CDKL5.

Despite no overall changes in gross dendritic morphology, we examined whether spine density was altered at basal, apical oblique or apical tuft dendrites (Fig. 9A).

We found a 19% increase in spine density in the basal dendrites of CA1 PCs from *Cdkl5*<sup>-/-</sup> rats (Fig. 9B, B', 19.18 ± 1.18 spines/10 μm) relative to WT controls (16.08 ± 0.98 spines/10 μm, LMM *p* = 0.04). Spine density did not differ between genotypes in the apical dendrites, oblique (Fig. 9C, C'; WT: 20.02 ± 1.76 spines/10 μm, *Cdkl5*<sup>-/-</sup>: 18.30 ± 0.92 spines/10 μm, LMM, *p* = 0.71) or tuft (Fig. 9D, D'; WT: 8.71 ± 0.78 spines/10 μm, *Cdkl5*<sup>-/-</sup>: 8.26 ± 0.82 spines/10 μm LMM *p* = 0.71).

### Unchanged relative abundance of silent synapses in *Cdkl5*<sup>-/-</sup> rats

To determine whether the reduced mEPSC frequency and increased spine density observed resulted from an increase in the relative abundance of NMDA receptor-only silent synapses, we used minimal stimulation of SC inputs to activate a single or a small number of synapses onto CA1, thus resulting in EPSCs or failures of synaptic transmission when recording AMPA receptor-mediated responses at a hyperpolarised holding potential (-70 mV). When the neuron is depolarised to +40 mV, mixed AMPA receptor and NMDA receptor-containing synapses as well as NMDA receptor-only containing synapses are activated (Fig. 10A, B). Under these conditions, the ratio of response probability at +40 mV relative to -70 mV allows for an estimation of the relative abundance of silent synapses [23]. When recording at -70 mV, response probability was similar for WT and *Cdkl5*<sup>-/-</sup> rats (WT:  $0.66 \pm 0.02$ , *Cdkl5*<sup>-/-</sup>  $0.73 \pm 0.03$ ,  $p=0.63$ ). The response probability increased similarly in both genotypes when recording at +40 mV (WT:  $0.79 \pm 0.03$ , *Cdkl5*<sup>-/-</sup>  $0.89 \pm 0.02$ ,  $p=0.21$  LMM), thus revealing the presence of silent synapses (Fig. 10C). The similar ratio of response probability across genotypes (Fig. 10D, WT:  $1.23 \pm 0.07$ ,

*Cdkl5*<sup>-/-</sup>  $1.21 \pm 0.08$ ,  $p=0.83$  GLMM) is consistent with low levels of silent synapses in CA1 pyramidal cells [48] and indicates that the abundance of silent synapses is unaltered in the absence of CDKL5. Overall, these data suggest that altered abundance of silent synapses does not contribute to the LTP and mEPSC phenotypes observed in *Cdkl5*<sup>-/-</sup> rats.

### Discussion

In this study we described and validated a novel rat model of CDD, whereby targeting exon 8 of the *Cdkl5* gene resulted in complete absence of CDKL5 protein. Extracellular field recordings revealed enhanced LTP in the hippocampus of *Cdkl5*<sup>-/-</sup> rats. However, extensive electrophysiological and biochemical characterization of NMDA receptors and AMPA receptors revealed no alteration in the functional properties of these receptors or the expression of their respective subunits. Further analysis of synaptic transmission in *Cdkl5*<sup>-/-</sup> rats revealed a reduction in mEPSC frequency however, this finding was not accompanied by a change in PPR or an altered expression of hippocampal presynaptic proteins. Morphological characterisation of CA1 PCs with Sholl analysis revealed typical dendritic branching in *Cdkl5*<sup>-/-</sup> rats.

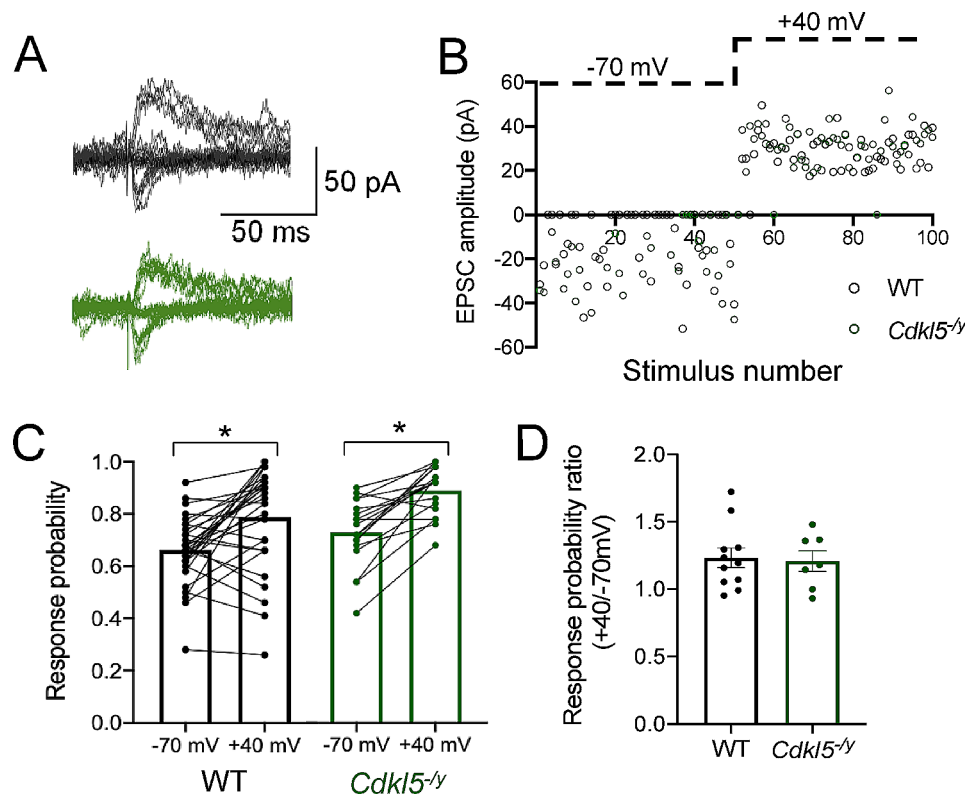


**Fig. 10** Minimal stimulation of CA3 inputs to CA1 pyramidal cells reveal no difference in silent synapses in *Cdkl5*<sup>-/-</sup> rats. **(A)** Representative traces of EPSCs recorded at -70 mV and +40 mV evoked by minimal stimulation of Schaffer collaterals. **(B)** Example time-course of synaptic responses throughout a single WT and *Cdkl5*<sup>-/-</sup> recording upon Schaffer collateral stimulation. **(C)** Response probability at -70 mV and +40 mV (data shown as cells, values for each cell connected by a black line). Two-way ANOVA Genotype effect:  $F_{1,46} = 5.16$ ,  $p=0.03$ , Holding potential effect:  $F_{1,46}=38.50$ ,  $p<0.0001$ ). **(D)** Ratio of the response probability at +40mV and -70 mV following minimal stimulation of Schaffer collaterals. (WT  $n = 30$  cells / 11 rats, *Cdkl5*<sup>-/-</sup>  $n = 18$  cells / 7 rats)

However, spine density was altered in a dendritic domain specific manner, with basal dendrites exhibiting higher spine density in *Cdkl5*<sup>-/-</sup> rats relative to WT, while spine density was unchanged in apical dendrites. Despite this increase in spine density and reduced mEPSC frequency, minimal stimulation experiments revealed unaltered abundance of silent synapses in *Cdkl5*<sup>-/-</sup> rats. Cellular excitability was also largely unaffected in the absence of CDKL5.

### **Mechanisms underlying enhanced hippocampal LTP are not conserved across mouse and rat models of CDD**

In this study we found enhanced LTP in the hippocampus of *Cdkl5*<sup>-/-</sup> rats, suggesting a role of CDKL5 in synaptic plasticity in this brain region. Whilst enhanced LTP has previously been reported in mouse models of CDD [12, 13], the mechanisms previously suggested to contribute to this phenotype in mice are not translated to the rat model used in this study. In contrast to [12], we did not observe alteration in NMDAR/AMPA ratio, NMDA receptor kinetics or subunit expression. Moreover, the developmental trajectory of NMDA receptor function and subunit expression can have long-lasting impact on circuit level function and had not yet been characterised in rodent models of CDD. In this study we show NMDA receptor development to be unaffected in *Cdkl5*<sup>-/-</sup> rats. The enhanced LTP is transitory as recordings from slices prepared from older *Cdkl5*<sup>-/-</sup> rats animals revealed no difference in its magnitude between genotypes. Whether the return to WT levels of LTP is brought about by the direct reversal of the mechanism which causes the early enhancement or is mediated by different processes is unclear and beyond the scope of the current study. Nevertheless, the reversal of the enhanced LTP in this CDD model indicates that during early development there is a complex interplay of signalling cascades that affect synaptic function.

Furthermore, our data do not show a difference between the rectification index for EPSCs recorded at negative and positive holding potentials which might be expected if the contribution of calcium permeable AMPA receptors differed between WT and *Cdkl5*<sup>-/-</sup> neuronal populations. We acknowledge this is contrary to what has been described in mouse models of CDD [13]. The overall linear I-V relationship of AMPA receptor mediated EPSCs observed in WT and *Cdkl5*<sup>-/-</sup> rats is also consistent with AMPA receptor populations being similar in both genotypes and is dominated by the known high expression of GluA2 subunit in CA1 PCs [36], which confers low calcium permeability and no inward rectification [49, 50]. We did observe a mixed inward and outward current in EPSCs recorded at 0 mV that might indicate the presence of calcium permeable AMPA receptors but these were observed in both WT and

*Cdkl5*<sup>-/-</sup> populations. While calcium permeable AMPA receptors have been associated with increased LTP in mouse models of CDD [13] and other unrelated mouse mutants [51], these were associated with increased calcium permeable AMPA receptors at baseline, which we did not observe here, supporting that this is not a mechanism of increased LTP in *Cdkl5*<sup>-/-</sup> compared to WT rats. The mechanisms that underlie inward rectification also involve the association of AMPA receptors with auxiliary subunits [52], however this may [53] or may not [54] depend on the specific auxiliary subunit ( $\gamma 2$  versus  $\gamma 8$ ); future studies are necessary to investigate any alterations in auxiliary subunits in *Cdkl5*<sup>-/-</sup> rodent models.

In addition to species differences, other factors can contribute to the discrepancies observed between our findings and previous studies. Namely the ages of the animals tested and the nature of the genetic alteration leading to lack of CDKL5. In this study we focused on early post-natal development (P7 onwards) and juvenile ages (P28-35) due to the neurodevelopmental nature of CDD. However, the vast majority of studies conducted in pre-clinical models of CDD have focused on adult mice (i.e. older than 2 months [10–12, 14, 15, 55]). Moreover, altered NMDA receptor function has been reported in a constitutive knock out of *Cdkl5* achieved by targeting exon 2 [12], CP-AMPA receptors have been implicated in the R59X mutation knock in mouse model [13], whilst the rat model used in this study results from targeting exon 8. Interestingly, discrepancies in behavioural phenotypes have been described across the variety of mouse models generated so far [56].

Our findings suggest ionotropic glutamate receptor function and expression of synaptic proteins is intact in *Cdkl5*<sup>-/-</sup> rats, therefore the cellular mechanisms underlying enhanced LTP in the rat model of CDD are yet to be understood. Work elucidating CDKL5 targets is still ongoing and currently there is little evidence that CDKL5 directly regulates signalling cascades downstream from LTP induction. Proteomic analyses did not reveal obvious effectors underlying enhanced LTP. Recent work utilizing a CDKL5-specific kinase inhibitor demonstrated reduced hippocampal LTP [57] which suggests unknown rodent specific compensations to genetic loss of *Cdkl5*. That said, downregulation of the mTOR signalling pathway has been reported across different mouse models of CDD [10, 55, 58]. Furthermore, altered mTOR signalling has been implicated in various other models of ASD/ID which also present with synaptic plasticity phenotypes (reviewed in [59]), as such examination of this pathway might provide insight into a potential mechanism for the synaptic plasticity phenotype in *Cdkl5*<sup>-/-</sup> rats.

### Excitatory synaptic transmission

In this study we report a reduction in mEPSC frequency in *Cdkl5*<sup>-/-</sup> rats. mEPSCs are synaptic neurotransmitter release events resulting from the stochastic fusion of single synaptic vesicles. Whilst mEPSC amplitude is a proxy for the number of receptors in the postsynaptic membrane, mEPSC frequency is a correlate for presynaptic release probability and/or synapse numbers. PPR is typically used to infer about presynaptic release probability [41, 60], however the relationship between PPR and release probability is complex, with studies showing that PPR can be maintained even when release probability is altered [61, 62]. In this study we find PPR to be unaltered at Schaffer collateral synapses in CA1 in *Cdkl5*<sup>-/-</sup> rats. One suggestion for this apparent contradiction is that the fusogenicity of individual synaptic vesicles in *Cdkl5*<sup>-/-</sup> synapses is unaltered, but the number of vesicles accessible for mEPSC events is reduced. This is supported by recent data from this *Cdkl5*<sup>-/-</sup> model system, in which the reformation of synaptic vesicles is perturbed after their fusion [63]. Regardless, the absence of effect on PPR coupled with the unaltered expression levels of presynaptic proteins, suggest that release probability is unlikely to be affected in the hippocampus of *Cdkl5*<sup>-/-</sup> rats.

As the reduction in mEPSC frequency was accompanied by an increase in spine density in basal dendrites, we used minimal stimulation to address the hypothesis that *Cdkl5*<sup>-/-</sup> rats exhibit a greater abundance of silent synapses. Furthermore, altered abundance of silent synapses has previously been suggested to underlie abnormal synaptic plasticity in other models of ASD/ID with co-occurring epilepsy [22]. The response probability observed upon minimal stimulation of SC inputs to CA1 was consistent with the prevalence of silent synapses expected for CA1, based on anatomical studies [48], but no genotypic differences were found, indicating that the reduction in mEPSC frequency we observe cannot be explained by an increase in functionally silent synapses. Similarly, we found no genotypic differences in the spine densities on apical dendrites of hippocampal neurons and a 15% increase on basal dendrites, however no synaptic markers were used to determine whether those spines are putative functional synapses. Therefore, it is plausible that despite the relatively small increase in overall spine density, *Cdkl5*<sup>-/-</sup> rats exhibit a reduction of functional synapses, explaining the reduction in mEPSC frequency observed. In support of this possibility, knock down of CDKL5 in neuronal cultures resulted in increased spine densities accompanied by a reduction in puncta of synaptic markers and reduced mEPSC frequency [39]. This is also supported by recent studies utilizing a CDKL5-specific kinase inhibitor [57].

### Limitations

This study has focussed on the electrophysiological and anatomical properties of hippocampal neurons across early postnatal development. Studies involving other brains regions, older animals and behavioural phenotypes associated with the loss of CDKL5 are needed to understand the pathophysiology of CDD. Furthermore, the contribution of this study was conducted in hemizygous male rats (where CDKL5 is completely absent) whilst most cases of CDD occur in heterozygous females. Clinically, the spectrum of severity is similar in males and females [64–66]. However, studying CDKL5 function in heterozygous females is complicated by the random X chromosome inactivation leading to mosaicism. The lack of reliable antibodies to identify CDKL5 positive and negative cells and the lack of reporter lines where this can be done in real time pose a significant obstacle to determine the role of CDKL5 in neuronal function in heterozygous females. Therefore, the study of hemizygous males can provide a useful tool to understand CDKL5 function in a simplified system.

Finally, the study of CDD in rodents has been clouded by the lack of a seizure phenotype in the models developed so far. Whilst children with CDD present with early-onset epilepsy [67], this feature of CDD is not translated to rodent models of the disorder [10, 12, 55], including the rat model described in this study. Indeed, spontaneous seizures have only been observed in aged heterozygous female mice (>300 days), with the burden of epileptic spasms depending on the nature of the genetic alteration [68]. The lack of a seizure phenotype in ours and other models generated thus far limits these models to understanding the cellular alterations in CDD. Furthermore, CDKL5 protein function is still poorly understood and rodent models can provide a useful tool to understanding the role of CDKL5 in neurons at the molecular and cellular level.

### Conclusion

This study described a novel rat model of CDD, of value to understand the role of CDKL5 in neurodevelopment in rodents. Moreover, the generation of this rat model provides a valuable tool to the CDD research community. In combination with the existing mouse models, the *Cdkl5*<sup>-/-</sup> rat can be used to identify robust cross species phenotypes that can be used as biomarkers when assessing potential therapeutics in preclinical models of CDD.

This study provides renewed evidence of a role of CDKL5 in excitatory synaptic transmission and synaptic plasticity in the hippocampus however the underlying mechanisms by which loss CDKL5 results in enhanced LTP and reduced mEPSC frequency remain to be elucidated.

## Abbreviations

ACSF	Artificial cerebral spinal fluid
AMPA	$\alpha$ -amino-3-hydroxy-5-methyl-4-isoxazolepropionic acid
ANOVA	Analysis of variance
ASD	Autism spectrum disorder
CDD	Cyclin-dependent kinase-like 5 deficiency disorder
CDKL5	cyclin-dependent kinase-like 5
CP	Calcium-permeable
EPSC	Excitatory postsynaptic current
fEPSP	Field excitatory postsynaptic potential
ID	Intellectual disability
LTP	Long-term potentiation
NMDA	<i>N</i> -methyl-D-aspartate
PC	Pyramidal cell
PPR	Paired-pulse ratio
SC	Schaffer collateral

## Supplementary Information

The online version contains supplementary material available at <https://doi.org/10.1186/s13229-024-00601-9>.

Supplementary Material 1  
Supplementary Material 2  
Supplementary Material 3  
Supplementary Material 4  
Supplementary Material 5  
Supplementary Material 6

## Author contributions

LSdO, HEO'L, SN, RL, ED, PB, SRL, OD, EP, EKO, GEH, MAC, SC, SAB, TAB, DJAW and PCK were responsible for the conception and design of the experiments. SN, OD, MAC, SC and PCK designed the CDKL5-*y* knock-out rat model. LSdO, HEO'L, SN, RL, ED, PB, SRL, MT, JP, OD and EP were responsible for the collection and assembly of data. LSdO, HEO'L, SN, RL, ED, PB, SRL, MY, JP, OD, EP, EKO, GEH, MAC, SC, SAB, TAB, DJAW and were responsible for the analysis and interpretation of data. LSdO, TAB, DJAW and PCK wrote the manuscript, and all authors had the opportunity to contribute to its editing. All persons designated as authors qualify for authorship, and all those who qualify for authorship are listed. All authors read and approved the final manuscript.

## Funding

TAB and HEO'L: NIH/NIMH T32 MH015442, International Foundation for CDKL5 Research, Loulou Foundation/U Penn Orphan Disease Center grant#CDKL5-17-101-01 and Ponzio Family Research Chair in Neurology Research (Children's Hospital Foundation); PCK: Loulou Foundation (no grant code number) and the SFARI (529085). MAC: Wellcome Trust Investigator Award to MAC (204954/Z/16/Z).

## Data availability

The datasets used and/or analysed during the current study are available from the corresponding author on reasonable request.

## Declarations

### Ethics approval and consent to participate

Not applicable.

### Consent for publication

Not applicable.

### Competing interests

The authors declare no competing interests.

### Author details

<sup>1</sup>Centre for Discovery Brain Sciences, University of Edinburgh, Edinburgh, UK

<sup>2</sup>Simons Initiative for the Developing Brain, Patrick Wild Centre, University of Edinburgh, Edinburgh, UK

<sup>3</sup>School of Medicine, University of Colorado, Denver, CO, USA

<sup>4</sup>National Centre for Biological Sciences, Tata Institute for Fundamental Research, Bangalore 560065, India

<sup>5</sup>Centre for Brain Development and Repair, Instem, Bangalore, India

<sup>6</sup>UK Dementia Research Institute, University of Edinburgh, Edinburgh, UK

<sup>7</sup>Faculty of Medical Sciences, Newcastle University Biosciences Institute, Newcastle upon Tyne NE2 4HH, UK

<sup>8</sup>Department of Pharmacology, University of Colorado Denver, 12800 East 19th Ave, Aurora, CO 80045, USA

<sup>9</sup>Centre for Discovery Brain Sciences, Simons Initiative for the Developing Brain, University of Edinburgh, Hugh Robson Building, Edinburgh EH8 9XD, UK

Received: 3 November 2023 / Accepted: 7 May 2024

Published online: 14 June 2024

## References

1. Olson HE, Demarest ST, Pestana-Knight EM, Swanson LC, Iqbal S, Lal D, Leonard H, Cross JH, Devinsky O, Benke TA. Cyclin-dependent kinase-like 5 Deficiency Disorder: clinical review. *Pediatr Neurol*. 2019;97:18–25.
2. Fehr S, Wilson M, Downs J, Williams S, Murgia A, Sartori S, Vecchi M, Ho G, Polli R, Psoni S, et al. The CDKL5 disorder is an independent clinical entity associated with early-onset encephalopathy. *Eur J Hum Genet*. 2013;21(3):266–73.
3. Hector RD, Kalscheuer VM, Hennig F, Leonard H, Downs J, Clarke A, Benke TA, Armstrong J, Pineda M, Bailey MES, et al. CDKL5 variants: improving our understanding of a rare neurologic disorder. *Neurol Genet*. 2017;3(6):e200.
4. Hector RD, Dando O, Landsberger N, Kilstrup-Nielsen C, Kind PC, Bailey ME, Cobb SR. Characterisation of CDKL5 transcript isoforms in Human and Mouse. *PLoS ONE*. 2016;11(6):e0157758.
5. Hector RD, Dando O, Ritakari TE, Kind PC, Bailey ME, Cobb SR. Characterisation of Cdkl5 transcript isoforms in rat. *Gene*. 2017;603:21–6.
6. Munoz IM, Morgan ME, Peltier J, Weiland F, Gregorczyk M, Brown FC, Macartney T, Toth R, Trost M, Rouse J. Phosphoproteomic screening identifies physiological substrates of the CDKL5 kinase. *EMBO J* 2018, 37(24).
7. Baltussen LL, Negraes PD, Silvestre M, Claxton S, Moeskops M, Christodoulou E, Flynn HR, Snijders AP, Muotri AR, Ulltanir SK. Chemical genetic identification of CDKL5 substrates reveals its role in neuronal microtubule dynamics. *EMBO J*. 2018;37(24).
8. Della Sala G, Putignano E, Chelini G, Melani R, Calcagno E, Michele Ratto G, Amendola E, Gross CT, Giustetto M, Pizzorusso T. Dendritic spine instability in a mouse model of CDKL5 disorder is rescued by insulin-like growth factor 1. *Biol Psychiatry*. 2016;80(4):302–11.
9. Fuchs C, Trazzi S, Torricella R, Viggiano R, De Franceschi M, Amendola E, Gross C, Calza L, Bartesaghi R, Ciani E. Loss of CDKL5 impairs survival and dendritic growth of newborn neurons by altering AKT/GSK-3 $\beta$  signaling. *Neurobiol Dis*. 2014;70(100):53–68.
10. Amendola E, Zhan Y, Mattucci C, Castroflorio E, Calcagno E, Fuchs C, Lonetti G, Silingardi D, Vyssotski AL, Farley D, et al. Mapping pathological phenotypes in a mouse model of CDKL5 disorder. *PLoS ONE*. 2014;9(5):e91613.
11. Tang S, Wang IJ, Yue C, Takano H, Terzic B, Pance K, Lee JY, Cui Y, Coulter DA, Zhou Z. Loss of CDKL5 in glutamatergic neurons disrupts hippocampal microcircuitry and leads to memory impairment in mice. *J Neurosci*. 2017;37(31):7420–37.
12. Okuda K, Kobayashi S, Fukaya M, Watanabe A, Murakami T, Hagiwara M, Sato T, Ueno H, Ogonuki N, Komano-Inoue S, et al. CDKL5 controls postsynaptic localization of GluN2B-containing NMDA receptors in the hippocampus and regulates seizure susceptibility. *Neurobiol Dis*. 2017;106:158–70.
13. Yennawar M, White RS, Jensen FE. AMPA receptor dysregulation and therapeutic interventions in a mouse model of CDKL5 Deficiency Disorder. *J Neurosci*. 2019;39(24):4814–28.
14. Tang S, Terzic B, Wang IJ, Sarmiento N, Sizov K, Cui Y, Takano H, Marsh ED, Zhou Z, Coulter DA. Altered NMDAR signaling underlies autistic-like features in mouse models of CDKL5 deficiency disorder. *Nat Commun*. 2019;10(1):2655.
15. Okuda K, Takao K, Watanabe A, Miyakawa T, Mizuguchi M, Tanaka T. Comprehensive behavioral analysis of the Cdkl5 knockout mice revealed significant enhancement in anxiety- and fear-related behaviors and impairment in both

- acquisition and long-term retention of spatial reference memory. *PLoS ONE*. 2018;13(4):e0196587.
16. Luthi A, Schwyzler L, Mateos JM, Gahwiler BH, McKinney RA. NMDA receptor activation limits the number of synaptic connections during hippocampal development. *Nat Neurosci*. 2001;4(11):1102–7.
  17. Hall BJ, Ripley B, Ghosh A. NR2B signaling regulates the development of synaptic AMPA receptor current. *J Neurosci*. 2007;27(49):13446–56.
  18. Oliveira LS, Sumera A, Booker SA. Repeated whole-cell patch-clamp recording from CA1 pyramidal cells in rodent hippocampal slices followed by axon initial segment labeling. *STAR Protoc*. 2021;2(1):100336.
  19. Komiyama NH, Watabe AM, Carlisle HJ, Porter K, Charlesworth P, Monti J, Strathdee DJ, O'Carroll CM, Martin SJ, Morris RG, et al. SynGAP regulates ERK/MAPK signaling, synaptic plasticity, and learning in the complex with post-synaptic density 95 and NMDA receptor. *J Neurosci*. 2002;22(22):9721–32.
  20. Anderson WW, Collingridge GL. Capabilities of the WinLTP data acquisition program extending beyond basic LTP experimental functions. *J Neurosci Methods*. 2007;162(1–2):346–56.
  21. Adesnik H, Nicoll RA. Conservation of glutamate receptor 2-containing AMPA receptors during long-term potentiation. *J Neurosci*. 2007;27(17):4598–602.
  22. Harlow EG, Till SM, Russell TA, Wijetunge LS, Kind P, Contractor A. Critical period plasticity is disrupted in the barrel cortex of FMR1 knockout mice. *Neuron*. 2010;65(3):385–98.
  23. Isaac JT, Crair MC, Nicoll RA, Malenka RC. Silent synapses during development of thalamocortical inputs. *Neuron*. 1997;18(2):269–80.
  24. Clements JD, Bekkers JM. Detection of spontaneous synaptic events with an optimally scaled template. *Biophys J*. 1997;73(1):220–9.
  25. Guzman SJ, Schlogl A, Schmidt-Hieber C. Stimfit: quantifying electrophysiological data with Python. *Front Neuroinform*. 2014;8:16.
  26. Dunkley PR, Jarvie PE, Robinson PJ. A rapid Percoll gradient procedure for preparation of synaptosomes. *Nat Protoc*. 2008;3(11):1718–28.
  27. Longair MH, Baker DA, Armstrong JD. Simple Neurite Tracer: open source software for reconstruction, visualization and analysis of neuronal processes. *Bioinformatics*. 2011;27(17):2453–4.
  28. Bates D, Machler M, Bolker BM, Walker SC. Fitting Linear mixed-effects models using lme4. *J Stat Softw*. 2015;67(1):1–48.
  29. Clement JP, Aceti M, Creson TK, Ozkan ED, Shi Y, Reish NJ, Almonte AG, Miller BH, Wiltgen BJ, Miller CA, et al. Pathogenic SYNGAP1 mutations impair cognitive development by disrupting maturation of dendritic spine synapses. *Cell*. 2012;151(4):709–23.
  30. Contractor A, Klyachko VA, Portera-Cailliau C. Altered neuronal and Circuit Excitability in Fragile X Syndrome. *Neuron*. 2015;87(4):699–715.
  31. Spruston N, Johnston D. Perforated patch-clamp analysis of the passive membrane properties of three classes of hippocampal neurons. *J Neurophysiol*. 1992;67(3):508–29.
  32. Staff NP, Jung HY, Thiagarajan T, Yao M, Spruston N. Resting and active properties of pyramidal neurons in subiculum and CA1 of rat hippocampus. *J Neurophysiol*. 2000;84(5):2398–408.
  33. Pickard L, Noel J, Henley JM, Collingridge GL, Molnar E. Developmental changes in synaptic AMPA and NMDA receptor distribution and AMPA receptor subunit composition in living hippocampal neurons. *J Neurosci*. 2000;20(21):7922–31.
  34. Flint AC, Maisch US, Weishaupt JH, Kriegstein AR, Monyer H. NR2A subunit expression shortens NMDA receptor synaptic currents in developing neocortex. *J Neurosci*. 1997;17(7):2469–76.
  35. Kamboj SK, Swanson GT, Cull-Candy SG. Intracellular spermine confers rectification on rat calcium-permeable AMPA and kainate receptors. *J Physiol*. 1995;486(Pt 2):297–303.
  36. He Y, Janssen WG, Morrison JH. Synaptic coexistence of AMPA and NMDA receptors in the rat hippocampus: a postembedding immunogold study. *J Neurosci Res*. 1998;54(4):444–9.
  37. Sekiguchi M, Katayama S, Hatano N, Shigeri Y, Sueyoshi N, Kameshita I. Identification of amphiphysin 1 as an endogenous substrate for CDKL5, a protein kinase associated with X-linked neurodevelopmental disorder. *Arch Biochem Biophys*. 2013;535(2):257–67.
  38. Nawaz MS, Giarda E, Bedogni F, La Montanara P, Ricciardi S, Ciceri D, Alberio T, Landsberger N, Rusconi L, Kilstrup-Nielsen C. CDKL5 and Shostin 1 interact and concur in regulating neuronal polarization. *PLoS ONE*. 2016;11(2):e0148634.
  39. Ricciardi S, Ungaro F, Hambrook M, Rademacher N, Stefanelli G, Brambilla D, Sessa A, Magagnotti C, Bachi A, Giarda E, et al. CDKL5 ensures excitatory synapse stability by reinforcing NGL-1-PSD95 interaction in the postsynaptic compartment and is impaired in patient iPSC-derived neurons. *Nat Cell Biol*. 2012;14(9):911–23.
  40. Fuchs C, Fustini N, Trazzi S, Gennaccaro L, Rimondini R, Ciani E. Treatment with the GSK3-beta inhibitor Tideglusib improves hippocampal development and memory performance in juvenile, but not adult, Cdk5 knockout mice. *Eur J Neurosci*. 2018;47(9):1054–66.
  41. Debanne D, Guerineau NC, Gahwiler BH, Thompson SM. Paired-pulse facilitation and depression at unitary synapses in rat hippocampus: quantal fluctuation affects subsequent release. *J Physiol*. 1996;491(Pt 1):163–76.
  42. Holmqvist MH, Cao J, Hernandez-Pineda R, Jacobson MD, Carroll KI, Sung MA, Betty M, Ge P, Gilbride KJ, Brown ME, et al. Elimination of fast inactivation in Kv4 A-type potassium channels by an auxiliary subunit domain. *Proc Natl Acad Sci U S A*. 2002;99(2):1035–40.
  43. Morohashi Y, Hatano N, Ohya S, Takikawa R, Watabiki T, Takasugi N, Imaizumi Y, Tomita T, Iwatsubo T. Molecular cloning and characterization of CALP/kChIP4, a novel EF-hand protein interacting with presenilin 2 and voltage-gated potassium channel subunit Kv4. *J Biol Chem*. 2002;277(17):14965–75.
  44. Vetter P, Roth A, Hausser M. Propagation of action potentials in dendrites depends on dendritic morphology. *J Neurophysiol*. 2001;85(2):926–37.
  45. Mainen ZF, Sejnowski TJ. Influence of dendritic structure on firing pattern in model neocortical neurons. *Nature*. 1996;382(6589):363–6.
  46. Amaral DG, Witter MP. The three-dimensional organization of the hippocampal formation: a review of anatomical data. *Neuroscience*. 1995;31(3):571–91.
  47. Bannister NJ, Larkman AU. Dendritic morphology of CA1 pyramidal neurones from the rat hippocampus: I. branching patterns. *J Comp Neurol*. 1995;360(1):150–60.
  48. Racca C, Stephenson FA, Streit P, Roberts JD, Somogyi P. NMDA receptor content of synapses in stratum radiatum of the hippocampal CA1 area. *J Neurosci*. 2000;20(7):2512–22.
  49. Jonas P, Racca C, Sakmann B, Seeburg PH, Monyer H. Differences in Ca<sup>2+</sup> permeability of AMPA-type glutamate receptor channels in neocortical neurons caused by differential GluR-B subunit expression. *Neuron*. 1994;12(6):1281–9.
  50. Jonas P, Sakmann B. Glutamate receptor channels in isolated patches from CA1 and CA3 pyramidal cells of rat hippocampal slices. *J Physiol*. 1992;455:143–71.
  51. Sanderson JL, Gorski JA, Dell'Acqua ML. NMDA receptor-dependent LTD requires transient synaptic incorporation of ca(2)(+)-Permeable AMPARs mediated by AKAP150-Anchored PKA and Calcineurin. *Neuron*. 2016;89(5):1000–15.
  52. Hansen KB, Wollmuth LP, Bowie D, Furukawa H, Menniti FS, Sobolevsky AI, Swanson GT, Swanger SA, Greger IH, Nakagawa T, et al. Structure, function, and pharmacology of glutamate receptor ion channels. *Pharmacol Rev*. 2021;73(4):298–487.
  53. Soto D, Coombs ID, Kelly L, Farrant M, Cull-Candy SG. Stargazin attenuates intracellular polyamine block of calcium-permeable AMPA receptors. *Nat Neurosci*. 2007;10(10):1260–7.
  54. Rouach N, Byrd K, Petralia RS, Elias GM, Adesnik H, Tomita S, Karimzadegan S, Kealey C, Bredt DS, Nicoll RA. TARP gamma-8 controls hippocampal AMPA receptor number, distribution and synaptic plasticity. *Nat Neurosci*. 2005;8(11):1525–33.
  55. Wang IT, Allen M, Goffin D, Zhu X, Fairless AH, Brodwin ES, Siegel SJ, Marsh ED, Blendy JA, Zhou Z. Loss of CDKL5 disrupts kinome profile and event-related potentials leading to autistic-like phenotypes in mice. *Proc Natl Acad Sci U S A*. 2012;109(52):21516–21.
  56. Zhu YC, Xiong ZQ. Molecular and synaptic bases of CDKL5 disorder. *Dev Neurobiol*. 2019;79(1):8–19.
  57. Castano A, Silvestre M, Wells CI, Sanderson JL, Ferrer CA, Ong HW, Lang Y, Richardson W, Silvaroli JA, Bashore FM et al. Discovery and characterization of a specific inhibitor of serine-threonine kinase cyclin-dependent kinase-like 5 (CDKL5) demonstrates role in hippocampal CA1 physiology. *Elife* 2023, 12.
  58. Schroeder E, Yuan L, Seong E, Ligon C, DeKover N, Gurumurthy CB, Arikath J. Neuron-type specific loss of CDKL5 leads to alterations in mTOR Signaling and synaptic markers. *Mol Neurobiol*. 2019;56(6):4151–62.
  59. Winden KD, Ebrahimi-Fakhari D, Sahin M. Abnormal mTOR activation in Autism. *Annu Rev Neurosci*. 2018;41:1–23.
  60. Dobrunz LE, Stevens CF. Heterogeneity of release probability, facilitation, and depletion at central synapses. *Neuron*. 1997;18(6):995–1008.
  61. Manita S, Suzuki T, Inoue M, Kudo Y, Miyakawa H. Paired-pulse ratio of synaptically induced transporter currents at hippocampal CA1 synapses is not related to release probability. *Brain Res*. 2007;1154:71–9.

62. Burke KJ Jr, Keeshen CM, Bender KJ. Two forms of synaptic Depression produced by Differential Neuromodulation of presynaptic calcium channels. *Neuron*. 2018;99(5):969–84. e967.
63. Kontaxi C, Ivanova D, Davenport EC, Kind PC, Cousin MA. Epilepsy-Related CDKL5 Deficiency slows synaptic vesicle endocytosis in central nerve terminals. *J Neurosci*. 2023;43(11):2002–20.
64. Demarest ST, Olson HE, Moss A, Pestana-Knight E, Zhang X, Parikh S, Swanson LC, Riley KD, Bazin GA, Angione K, et al. CDKL5 deficiency disorder: relationship between genotype, epilepsy, cortical visual impairment, and development. *Epilepsia*. 2019;60(8):1733–42.
65. MacKay CI, Wong K, Demarest ST, Benke TA, Downs J, Leonard H. Exploring genotype-phenotype relationships in the CDKL5 deficiency disorder using an international dataset. *Clin Genet*. 2021;99(1):157–65.
66. Siri B, Varesio C, Freri E, Darra F, Gana S, Mei D, Porta F, Fontana E, Galati G, Solazzi R, et al. CDKL5 deficiency disorder in males: five new variants and review of the literature. *Eur J Paediatr Neurol*. 2021;33:9–20.
67. Bahi-Buisson N, Bienvenu T. CDKL5-Related disorders: from clinical description to Molecular Genetics. *Mol Syndromol*. 2012;2(3–5):137–52.
68. Mulcahey PJ, Tang S, Takano H, White A, Davila Portillo DR, Kane OM, Marsh ED, Zhou Z, Coulter DA. Aged heterozygous Cdkl5 mutant mice exhibit spontaneous epileptic spasms. *Exp Neurol*. 2020;332:113388.

### Publisher's Note

Springer Nature remains neutral with regard to jurisdictional claims in published maps and institutional affiliations.